

optical data for selenium by inspection of the energy bands alone has led to quite erroneous results,^{2,8} especially since those bands were only known at a few symmetry points and axes. Early calculations^{1,2} included merely the Δ axis and consequently tried to explain the reflectivity spectrum in terms of this single axis. However, Fig. 8 shows that this axis contributes very little, because the oscillator strengths are in general quite small.

Because the bands are flat, it was found that a decomposition of ϵ_2 into contributions from different bands rather than different regions in k space provides somewhat more understanding at least of the basic structure. Here the ultraviolet measurements of Mohler *et al.*⁷ were most helpful as a test on our interpretation. More experimental work using modern differential techniques (piezoreflectance²² or electroreflectance²³)

²² U. Gerhardt, Phys. Status Solidi **11**, 801 (1965).

²³ B. O. Seraphin and N. Bottka, Phys. Rev. **145**, 628 (1966).

could, in the future, bring additional information about the location of certain transitions in the Brillouin zone—provided they are at all localized.

ACKNOWLEDGMENTS

This work was supported by the U. S. Army Research Office (Durham) and in part by the U. S. Atomic Energy Commission. I have further used facilities provided by the Advanced Research Projects Agency for materials research at the University of Chicago. The numerical calculations were carried out at the Computer Centers of the University of Chicago and the Argonne National Laboratory, whose services are appreciated. I wish to express my gratitude to Professor J. C. Phillips and Dr. Fred M. Mueller for numerous fruitful suggestions and advice. I have also benefitted from discussions with Professor M. H. Cohen, Professor David Brust, Dr. U. Gerhardt, and Dr. T. Bergstresser.

Photoemission Study of the Electronic Structure of Wurtzite CdSe and CdS*

J. L. SHAY† AND W. E. SPICER

Stanford Electronics Laboratories, Stanford University, Stanford, California

(Received 5 October 1967)

In photoemission studies of single crystals of CdSe and CdS cleaved in vacuum, structure due to both direct transitions (\mathbf{k} conserved) and nondirect transitions (\mathbf{k} not important) is found. We explicitly separate the contributions to the energy distributions of the photoemitted electrons due to direct transitions from those due to nondirect transitions. By correlating structure in the energy distributions with structure in the reflectivity we determine (1) the energy of the initial and final states for the transitions causing this structure, and (2) the nature of the transitions (direct or nondirect or a combination of both). For CdSe we find that the transitions resulting in the E_2 reflectivity peak are direct and have initial states near -1.6 eV and final states near 5.8 eV (both with respect to the valence-band maximum). By comparing these initial and final states with the pseudopotential band structure of Bergstresser and Cohen, we find that these transitions occur at regions of the Brillouin zone around H and K . The E_1' reflectivity peak is due to direct transitions from initial states near -0.9 eV to final states near 7.5 eV; however, the region of the Brillouin zone involved is not certain. Whereas we show that the E_2 structure is almost entirely due to direct transitions, only about 20% of the absorption near the E_1' peak is due to direct transitions, the other 80% being due to nondirect transitions. We suggest that the F_3 reflectivity shoulder is due to nondirect transitions from a peak at -1.3 eV in the valence-band optical density of states to a peak at 7.5 eV in the conduction-band effective optical density of states. The nondirect transitions from this valence-band peak at -1.3 eV (and to this conduction-band peak at 7.5 eV) are observed over a wide range of photon energy. Direct transitions from initial states near the valence-band maximum are observed for $\hbar\omega \gtrsim 10.2$ eV. This suggests that there is a Γ conduction band near 10.2 eV. A deep valence band, tentatively identified as the cadmium $4d$ band, has been located at -9.9 eV. The results for CdS are similar, except that the relevant conduction-band states lie ~ 0.5 eV higher than in CdSe.

I. INTRODUCTION

THE purpose of this study has been to use photoemission techniques to investigate the electronic structure of wurtzite CdSe and CdS over a wide energy

range. One of the principal advantages of the photoemission experiment is that it allows the determination of the absolute energies of the initial and final states for strong electronic transitions; conventional optical

* This work was supported by the National Aeronautics and Space Administration and the Advanced Research Projects Agency through the Center for Materials Research at Stanford

and was based on a Ph.D. dissertation by J. L. Shay, Stanford University, 1966 (unpublished).

† Present address: Bell Telephone Laboratories, Holmdel, N. J.

experiments measure only the energy differences between quantum levels.

Photoemission data can also be used to determine the nature of an electronic transition. Ordinary one-electron band theory requires conservation of wave vector in an optical transition. This selection rule causes the energy distributions of the photoemitted electrons to have distinctive characteristics which are readily observed experimentally.^{1,2} These characteristics are discussed in Sec. II. However, the energy distributions from a number of materials cannot be explained by direct transitions (see Sec. II). These latter studies find that sometimes conservation of wave vector does not provide an important selection rule. Characteristics of these nondirect transitions are also discussed in Sec. II. In the present studies we employ a method of data analysis which determines explicitly whether or not an optical transition is direct. When a transition is direct, the initial and final states determined from the photoemission data can be used in conjunction with a theoretical band structure to locate the region of the Brillouin zone making the dominant contribution to the transition probability.

The method for separating the direct and nondirect contributions to the energy distributions is discussed in Sec. II and the experimental techniques are described in Sec. III. In Secs. IV and V we present the photoemission studies of CdSe and CdS, respectively. In Sec. VI we discuss some of the effects of electron-electron scattering (pair production). Using an approximate expression for the quantum yield, we determine experimental values for the escape depth which is probably a rough measure of the mean free path for inelastic scattering (pair production).

II. THEORY AND METHODS FOR DATA ANALYSIS

If the initial and final states for an electronic transition are the one-electron states of band theory and if Koopmans's theorem applies, then the wave vector of the initial and final states must be practically identical. As discussed by Spicer,³ this selection rule causes the energy distributions of the photoemitted electrons, frequently referred to as energy distribution curves (EDC), to have features which allow the occurrence of these direct transitions to be detected. These features are summarized in Table I. The energy of the initial state varies with photon energy; and as a result, peaks in the EDC move with changes in energy unequal to the changes in photon energy. Furthermore, the strength of a transition is determined by the joint density of states; and as a result, structure appears and disappears in the EDC as $\hbar\omega$ is varied.

¹ J. L. Shay, W. E. Spicer, and Frank Herman, *Phys. Rev. Letters* **18**, 649 (1967).

² J. L. Shay and W. E. Spicer, *Phys. Rev.* **161**, 799 (1967).

³ W. E. Spicer, *Phys. Rev.* **154**, 385 (1967), and references therein.

TABLE I. Features of NEDC characteristic of direct and nondirect transitions.

Model	Features of NEDC
Direct transitions	Energy of initial state is a function of $\hbar\omega$; hence peaks move $\Delta(E_p) \neq \Delta(\hbar\omega)$. Strength determined by joint density of states; hence structure appears and disappears as $\hbar\omega$ is varied.
Nondirect transitions ^a	Strength determined by density-of-states product; peaks due to valence-band structure move $\Delta(E_p) = \Delta(\hbar\omega)$. Peaks due to conduction-band structure do not move.

^a The distinction between nondirect transitions and direct transitions between "flat" bands has been discussed in several places (Refs. 5 and 8).

Although ordinary one-electron band theory requires conservation of wave vector in an optical transition, the EDC from a number of materials³⁻⁸ cannot be explained by direct transitions. These studies find that conservation of wave vector is not an important selection rule, and for many of these materials a knowledge of the optical density of states (frequently referred to as ODS) is sufficient to predict the experimental EDC and optical data. Conversely, the optical density of states can be obtained from the EDC. These latter electronic transitions for which \mathbf{k} conservation is not an important selection rule are referred to as nondirect transitions. In addition to the density of conduction-band states, the conduction-band ODS that is derived from photoemission data will be influenced by the energy dependence of both the inelastic-scattering probability (pair production) and the threshold function (surface-transmission probability for photoexcited electrons approaching the surface). Since usually it is not possible to separate these latter effects from the true ODS, we shall refer to the conduction-band ODS that is deduced from photoemission data as the effective optical density of states (EODS). Since both the inelastic-scattering probability and the threshold function are usually smooth functions of electron energy, peaks in the EODS usually result from peaks in the true optical density of states. In our earlier studies of CdTe^{1,2} we referred to both the valence-band ODS and the conduction-band EODS as the "effective density of states."

Features of the EDC characteristic of nondirect transitions are also listed in Table I. Since the strength of a nondirect transition is determined by the product of the valence-band ODS and the conduction-band EODS, peaks in the EDC due to structure in the valence band move to higher energy with increments of energy equal to changes in photon energy, and peaks in the

⁴ N. B. Kindig and W. E. Spicer, *Solid State Commun.* **2**, 13 (1964).

⁵ N. B. Kindig and W. E. Spicer, *Phys. Rev.* **138**, A561 (1965).

⁶ W. E. Spicer, *J. Appl. Phys.* **37**, 949 (1966), and references therein.

⁷ W. E. Spicer, *Phys. Rev. Letters* **11**, 243 (1963).

⁸ C. N. Berglund and W. E. Spicer, *Phys. Rev.* **136**, A1030 (1964); **136**, A1044 (1964).

EDC due to structure in the conduction band do not move as the photon energy is varied.

Methods have been developed for separating the direct and nondirect contributions to the EDC and for determining the electronic density of states when the EDC result from nondirect transitions. Spicer⁷ was the first to derive a valence-band ODS from EDC. Berglund and Spicer⁸ analyzed materials in which the structure was predominantly in the valence band, and Kindig and Spicer⁵ developed a detailed method for cases in which strong structure occurs in both the conduction band and the valence band. The analysis used in the present work is due to Eden and Spicer.^{9,10} If the nondirect model is sufficient to explain the photoemission data, then the method used here derives the same ODS as do the earlier methods. When the photoemission data are due to a mixture of direct and nondirect transitions, the present method explicitly separates the portions of the EDC due to direct transitions from those due to nondirect transitions. The details of this analysis and an example of its application have been given elsewhere.²

III. EXPERIMENTAL METHODS

Many of the experimental methods used in this work have been reported previously¹¹⁻¹³ and for this reason they are only outlined here. The experiments have been performed at room temperature on single crystals of CdSe and CdS cleaved in vacuum. The cleavage was along planes parallel to the *C* axis. For both materials the most satisfactory cleavage plane is (1210). High-vacuum experiments were performed at pressures near 10^{-9} Torr using a modified version of the sample chamber and vacuum system described by Kindig and Spicer.¹² Other high-vacuum experiments used the sample chamber and vacuum system described by Powell.¹⁴ A magnetic shield¹³ was placed around the magnet used with the VacIon pump so that the chamber could be continuously pumped during an experiment with no distortion of the EDC due to the magnetic field.

In addition to these studies in high vacuum, several samples were also cleaved in the poorer vacuum of the McPherson monochromator, model 225. In these low-vacuum experiments there is no window between the light source and the cleaved crystal. Hence measurements can be extended beyond the 12 eV cutoff of the LiF window that seals the high-vacuum chamber. The

details of these low-vacuum experiments have been given elsewhere.^{2,13} A bonus of these low-vacuum experiments is that the electron affinity is about a volt lower than for a crystal cleaved in ultrahigh vacuum. In other experiments (see below) we have shown that the reduction in electron affinity is not caused by the gas flowing through the discharge lamp (pressure $\sim 10^{-4}$ Torr H₂) but by the background pressure of $\sim 10^{-7}$ Torr for this oil-diffusion pump system. Hence these low-vacuum experiments were performed at an "effective pressure" of $\sim 10^{-7}$ Torr. For photon energies well above threshold, there were more scattered electrons in the low-vacuum EDC than in the high-vacuum EDC at the same photon energies, but there were no other significant differences other than the difference in electron affinity. The difference in the number of scattered electrons is discussed in detail in Sec. VI.

The EDC were measured using the ac method described by Spicer and Berglund.¹¹ The estimated uncertainty in the location of structure in the EDC is ± 0.2 eV. Electron energies are stated relative to the top of the valence band. The absolute response of the Cs₃Sb phototube used for measuring light intensity was calibrated¹⁵ using a Reeder vacuum thermopile and sodium salicylate with an estimated uncertainty of $\pm 10\%$. The quantum yield is defined as the total number of photoemitted electrons per incident photon, and the EDC have been normalized by requiring that the area under an EDC equals the measured yield at that photon energy. Energy distributions that have been normalized to the yield will be called NEDC (normalized EDC).

We have performed experiments in which high-vacuum-cleaved samples of CdSe and CdS were exposed to as much as a $5\text{-}\mu$ pressure of ultrapure Linde hydrogen in the high-vacuum chamber. The yield and energy distributions measured while the samples were exposed to the hydrogen were indistinguishable from the measurements before the high-vacuum cleavages were exposed to the hydrogen. These experiments show conclusively that the lower electron affinity and increased number of secondary electrons which are observed in the low-vacuum measurements in the monochromator are neither due to hydrogen adsorbed on the surface nor to hydrogen that has diffused into the crystal.

IV. PHOTOEMISSION STUDY OF CdSe

A. Quantum Yield

We present in Fig. 1 the absolute quantum yields for a crystal of CdSe cleaved in high vacuum and for the same crystal cleaved in low vacuum. The electron affinity for the low-vacuum-cleaved sample is more than a volt lower than for the high-vacuum-cleaved sample. The low-vacuum yield is everywhere greater than the

¹⁵ Much of this calibration has been performed in our laboratory by Richard Koyama.

⁹ R. C. Eden and W. E. Spicer (to be published).

¹⁰ R. C. Eden, Ph.D. dissertation, Stanford University, 1967 (unpublished) [Solid State Electronics Laboratory Technical Report No. 5221-1, 1967 (unpublished)].

¹¹ W. E. Spicer and C. N. Berglund, *Rev. Sci. Instr.* **35**, 1665 (1964).

¹² N. B. Kindig and W. E. Spicer, *Rev. Sci. Instr.* **36**, 759 (1965).

¹³ J. L. Shay, Ph.D. dissertation, Stanford University, 1966 (unpublished) [Solid State Electronics Laboratory Technical Report No. 5216-1, 1966 (unpublished)].

¹⁴ R. J. Powell, Ph.D. dissertation, Stanford University, 1967 (unpublished) [Solid State Electronics Laboratory Technical Report No. 5220-1, 1967 (unpublished)].

high-vacuum yield, and for $\hbar\omega \gtrsim 9$ eV it shows a rise not present in the high-vacuum yield. Later, using NEDC, we show that this rise in yield is due to the escape of secondary electrons produced by pair production.

Since the threshold for photoemission from the high-vacuum-cleaved crystal is about 7 eV (Fig. 1) and the valence band is about 3 eV wide,¹⁶ all photoelectrons should have energies above the vacuum level for $\hbar\omega \gtrsim 10$ eV. Yet the yield in this region of photon energy is only about 7%. Although some electrons are probably reflected at the semiconductor surface, the small yield of 7% indicates that a large fraction of the photoexcited electrons are lost owing to electron-electron scattering (pair production) on their way to the surface. In Sec. VI we estimate the value of the escape depth.

B. Energy Distributions of the Photoemitted Electrons

1. Low-Vacuum Experiments

In Figs. 2-8 we present normalized energy distribution curves (NEDC) for a crystal cleaved in the vacuum of the monochromator (see Sec. III). Except for $\hbar\omega = 16.8$ and 21.2 eV, all curves have been normalized to the quantum yield. As the photon energy is increased above the threshold for photoemission, the first striking feature of the NEDC is the abrupt appearance of the peak *P1* for $\hbar\omega \leq 7.4$ eV (Figs. 2 and 3). The amplitude of peak *P1* is a maximum for $\hbar\omega = 7.4$ eV when it arises principally from transitions to final states near 5.8 eV from initial states centered at -1.6 eV. This abrupt appearance of *P1* in the NEDC corresponds to the E_2 reflectivity peak¹⁷ at 7.5 eV in Fig. 9 and the peak in $\epsilon_2\omega^2$ at 7.3 eV in Fig. 10. Hence the photoemission data indicate that the E_2 structure in the optical data is due principally to transitions to final states near 5.8 eV from initial states near -1.6 eV.

The increase in the valence-band density of states as the photon energy probes deeper into the valence band is insufficient to explain the abrupt appearance of *P1*. The valence band ODS which we deduce from the NEDC in Sec. IV C shows no such rapid rise. Rather we show in Sec. IV D that the abrupt appearance of *P1* in the NEDC is explained qualitatively by the pseudopotential band structure calculated by Bergstresser and Cohen.¹⁶ We conclude that *P1* and the associated E_2 reflectivity peak are due to direct transitions. However, our only proof that the abrupt appearance of *P1* is due to direct transitions rather than some other selection rule is the agreement with the theoretical band calculation.

For $\hbar\omega > 7.4$ eV, *P1* drops out of the NEDC and a small peak labeled DT is uncovered at energies near 6.5 eV (Figs. 4-6). DT moves to higher energies slightly with increasing photon energy, suggesting that DT is

¹⁶ T. Bergstresser and M. Cohen, Phys. Rev. **164**, 1069 (1967).

¹⁷ M. Cardona and G. Harbeke, Phys. Rev. **137**, A1467 (1965).

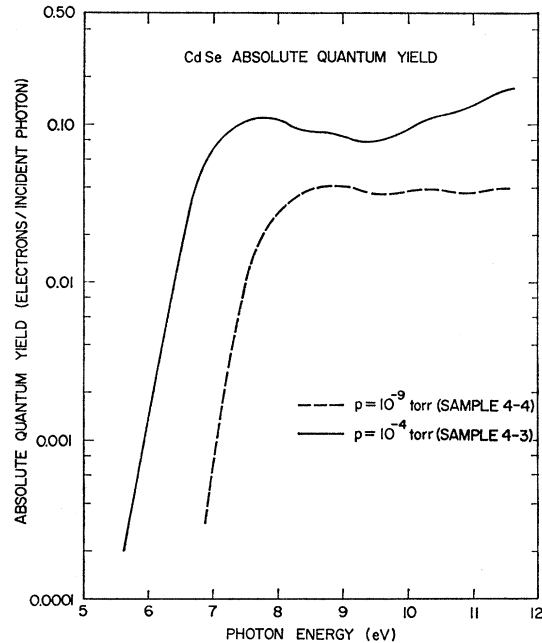


FIG. 1. Absolute quantum yields for a crystal of CdSe cleaved in high vacuum (pressure = 10^{-9} Torr) and in low vacuum (pressure = 10^{-4} Torr). The pressure of 10^{-4} Torr consists of hydrogen and a 10^{-7} Torr background pressure of the oil-diffusion pump. In another experiment (described in the text) we show that the reduced electron affinity in the low-vacuum experiment is entirely due to the background pressure of 10^{-7} Torr.

due to direct transitions (Table I). However, the region of the Brillouin zone producing this weak structure is not known.

For photon energies above about 7.6 eV two additional pieces of structure appear in the NEDC (Figs. 3-6). Peak CB appears at a fixed energy of 7.5 eV and is assigned to conduction-band structure; peak VB

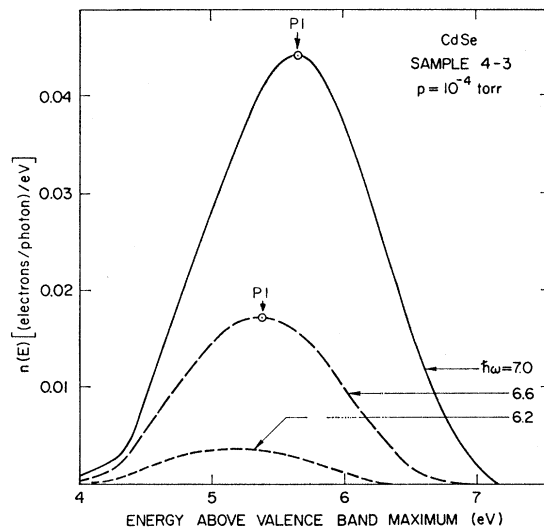


FIG. 2. Normalized energy distributions of the photoemitted electrons for the low-vacuum-cleaved crystal. $6.2 \leq \hbar\omega \leq 7.0$ eV.

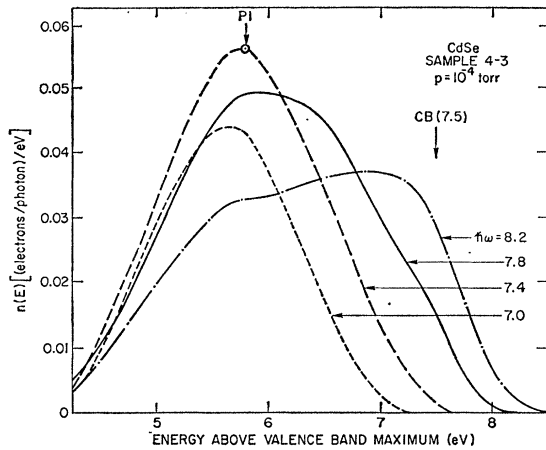


FIG. 3. Normalized energy distributions of the photoemitted electrons for the low-vacuum-cleaved crystal. $7.0 \leq \hbar\omega \leq 8.2$ eV.

moves to higher energies as the photon energy is increased and is assigned to valence-band structure. For a photon energy $\hbar\omega$ the location of VB is approximately given by

$$E_{VB} = \hbar\omega - 1.3 \text{ eV.} \quad (1)$$

The motion of VB in accordance with Eq. (1) indicates that it is due to nondirect transitions from a peak at -1.3 eV in the valence-band ODS, and thus that con-

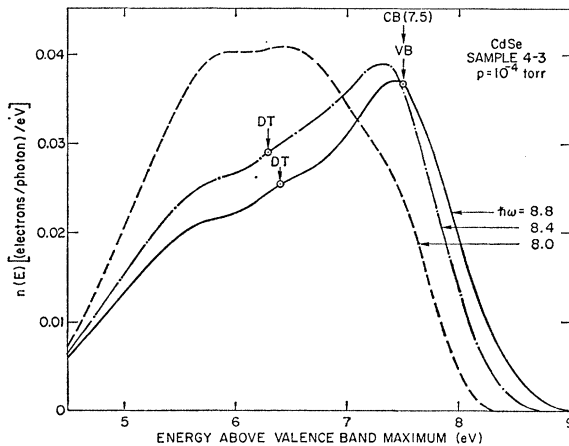


FIG. 4. Normalized energy distributions of the photoemitted electrons for the low-vacuum-cleaved crystal. $8.0 \leq \hbar\omega \leq 8.8$ eV.

servation of wave vector is not an important selection rule for the transitions associated with VB (Table I).

For a photon energy of 8.8 eV, the peak VB is coupled to the conduction-band structure CB at 7.5 eV. The corresponding features of the optical data are the E_1' reflectivity peak near 8.5 eV (Fig. 9) and the peak in $\epsilon_2\omega^2$ near 8.3 eV (Fig. 10). Although the peak VB coincides with the conduction-band structure CB for a photon energy of 8.8 eV, this portion of the NEDC has its maximum amplitude for a photon energy of 8.4 eV.

The detailed explanation for this apparent discrepancy of 0.4 eV is given in Sec. IV C; however, we outline it here. Through a detailed analysis of the NEDC, we find that although the nondirect transitions to conduction-band states near 7.5 eV are a maximum for $\hbar\omega = 8.8$ eV, there are a significant number of direct transitions to these same conduction-band states for $7.6 \lesssim \hbar\omega \lesssim 8.6$ eV.

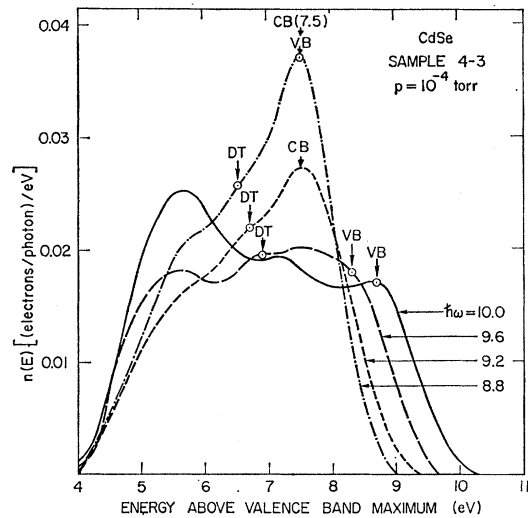


FIG. 5. Normalized energy distributions of the photoemitted electrons for the low-vacuum-cleaved crystal. $8.8 \leq \hbar\omega \leq 10.0$ eV.

The addition of the direct transitions to the more numerous nondirect transitions causes the amplitude of the NEDC to be a maximum for $\hbar\omega = 8.4$ eV. This also explains why $\epsilon_2\omega^2$ is a maximum near 8.3 eV although the nondirect transitions are strongest for $\hbar\omega = 8.8$ eV.

As VB moves to higher energies in accordance with Eq. (1) for $\hbar\omega > 8.8$ eV, the peak CB remains at 7.5 eV. This appearance of a peak at the same energy for all

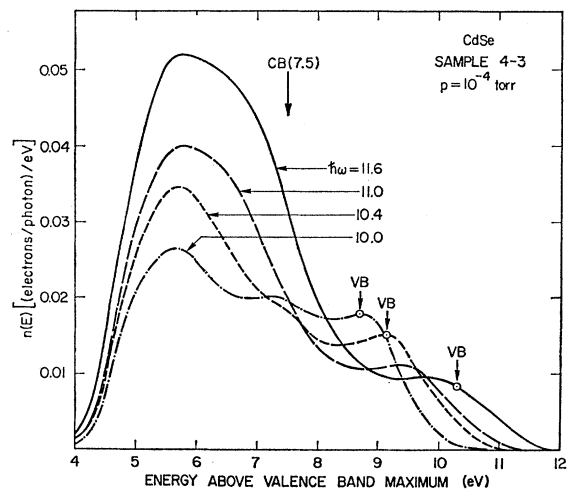


FIG. 6. Normalized energy distributions of the photoemitted electrons for the low-vacuum-cleaved crystal. $10.0 \leq \hbar\omega \leq 11.6$ eV.

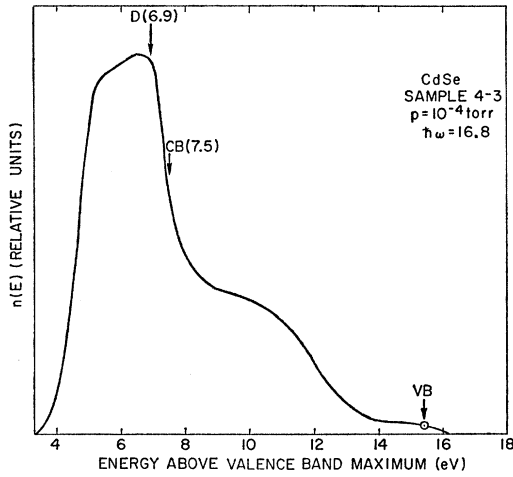


FIG. 7. Energy distribution of the photoemitted electrons for the low-vacuum-cleaved crystal. We suggest that peak D is due to transitions from the d -band density of states at -9.9 eV.

photon energies is characteristic of nondirect transitions to a peak in the conduction-band EODS (Table I).

The low-energy peak appearing in the NEDC for $\hbar\omega \gtrsim 9.6$ eV (Figs. 5–8) has the character expected from a peak due to secondary electrons created by pair production.^{8,18,19} As the photon energy is increased this peak rapidly overwhelms the primary photoelectrons so that by $\hbar\omega = 11$ eV, approximately 90% of the photoemission results from these scattered electrons. The

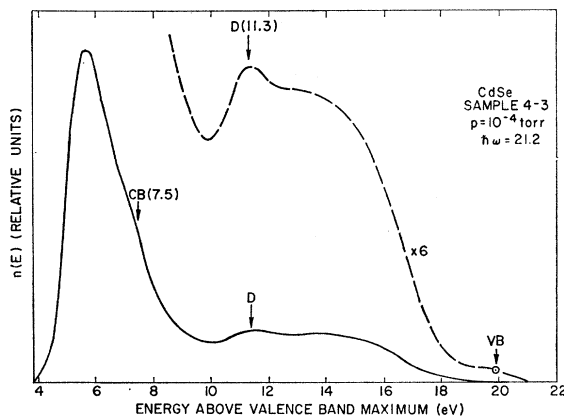


FIG. 8. Energy distribution of the photoemitted electrons for the low-vacuum-cleaved crystal. We suggest that peak D is due to transitions from the d -band density of states at -9.9 eV.

detailed shape of this scattering peak is not completely understood. In Sec. VI we discuss the difference in the scattering observed in the high- and low-vacuum experiments.

In Figs. 7 and 8 we present EDC for $\hbar\omega = 16.8$ and 21.2 eV. Most of the photoemitted electrons have been

inelastically scattered from higher energies. However, for $\hbar\omega = 21.2$ eV the peak of electrons labeled D at 11.3 eV in Fig. 8 is believed to be due to transitions from a high density of states at -9.9 eV in the valence band. We suggest that these valence-band states are derived from cadmium $4d$ states, since on the cadmium ion the $4d$ states lie about 9 eV below the $5s$ states.²⁰ We cannot rule out the possibility that peak D is due to the valence-band splitoff by about 10 eV from the

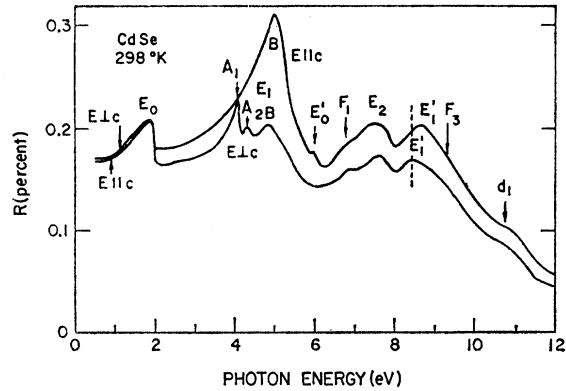


FIG. 9. Reflectivity of CdSe measured by Cardona and Harbeke (Ref. 17).

others. However, the density of states for this valence band is only 2 electrons per molecule, whereas there are 10 d electrons per molecule. It might be possible to establish the origin of peak D from optical data by applying a sum rule which relates total absorption to the number of electrons contributed by each molecule.²¹

It is not possible to follow the motion of peak D over a wide range of photon energy to confirm its origin

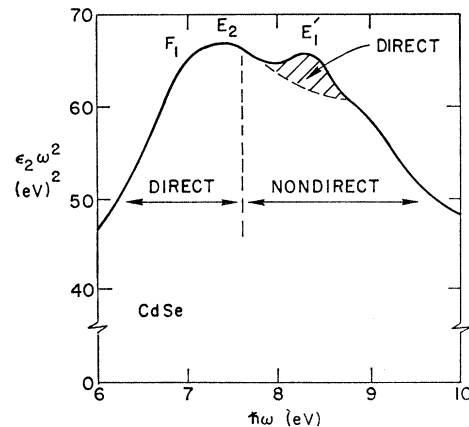


FIG. 10. The imaginary part of the dielectric function (ϵ_2) times the square of the photon energy. We evaluated this function using optical data obtained by Cardona and Harbeke (Ref. 17) from a Kramers-Kronig transform of their reflectance data. We indicate in this figure our estimate of the contributions of direct and nondirect transitions.

¹⁸ L. Apker, E. A. Taft, and J. Dickey, *J. Opt. Soc. Am.* **43**, 78 (1953).

¹⁹ W. E. Spicer, *J. Phys. Chem. Solids* **22**, 365 (1961).

²⁰ A similar suggestion has been made by Kindig and Spicer (Ref. 5) for the corresponding structure in CdS.

²¹ H. R. Phillip and H. Ehrenreich, *Phys. Rev.* **129**, 1550 (1963).

TABLE II. Correlation of photoemission and optical data for CdSe.

$\hbar\omega$ (eV)	Energy of final state ^a	Photoemission data ^a			Assignment suggested by this work	Reflectivity data ^b	
		Energy of initial state ^a	Nature of transition			$\hbar\omega$ (eV)	Label
7.4	5.8 (P1)	-1.6	Direct	Near zone edge connecting H & K	7.5 (7.5)	E_2	
8.4	~ 7.5	~ -0.9	Direct	Unknown	8.5 (8.3)	E_1'	
8.8	7.5 (CB)	-1.3 (VB)	Nondirect	Peaks in density of states	9.2 (9.0)	F_3	
$\gtrsim 8.0$	$\hbar\omega - 1.3$	-1.3 (VB)	Nondirect	Peak in valence-band density of states	
$\gtrsim 7.5$	7.5	...	Nondirect	Peak in conduction-band density of states	
7.6 to 10.6	6.3 to 7.8 (DT)	-1.3 to -2.8	Direct	Unknown	
...	...	-9.9 (D)	(Nondirect)	Transitions from d band	14	d_2	
>10.2	10.2 (S)	~ 0.0	Direct	Near Γ	10.7	d_1	

^a Labels in parentheses refer to structure in Figs. 2-8 and 11-14.

^b Reflectivity data (Fig. 9) are taken from Ref. 17. Numbers in parentheses are taken from the $\epsilon_{\infty}\omega^2$ plot in Fig. 10.

^c Energies are given in electron volts above the valence-band maximum. The estimated uncertainty in the location of peaks in the NEDC is ± 0.2 eV.

in the valence band; however, if the peak were due to conduction-band structure near 11.3 eV, we would expect to see a peak at 11.3 eV for $\hbar\omega = 16.8$ eV. No such peak is seen in Fig. 7. On the other hand, if the peak at 11.3 eV for $\hbar\omega = 21.2$ eV is in fact due to excitation from valence-band states near -9.9 eV, then for $\hbar\omega = 16.8$ eV this peak should be seen at 6.9 eV. The structure labeled D at 6.9 eV in Fig. 7 is believed to be due to these transitions. The d_2 reflectivity peak at 14 eV in Fig. 9 has been interpreted¹⁷ as resulting from transitions from the cadmium 4d band. Since the photoemission data have located these valence-band states at -9.9 eV, structure in the optical data near 14 eV is due to transitions to conduction-band states near 4.1 eV.

2. High-Vacuum Experiments

In Figs. 11-14 we present NEDC for a CdSe crystal cleaved in a vacuum of 10^{-9} Torr. The striking difference between these curves and the NEDC for the same crystal cleaved in the low-vacuum experiment is that the electron affinity is more than 1 eV larger for the high-vacuum cleavage. In addition, the number of scattered electrons appearing in the NEDC is smaller than for

the low-vacuum-cleaved sample (for further discussion see Sec. VI).

Most of the structure in high-vacuum data was also observed in the low-vacuum data and will not be discussed again. However a high-energy shoulder S is resolved in the high-vacuum NEDC for $\hbar\omega \gtrsim 10.2$ eV (Fig. 14). This shoulder is due to transitions from initial states near the top of the valence band to conduction-band states near 10.2 eV. The data are insufficient to determine unambiguously whether or not these are direct transitions, although the features of S are very similar to those of shoulders in the CdTe NEDC.^{1,2,13} The latter shoulders were shown to be due to direct transitions from the top of the valence band at Γ ($k=0$) to higher lying Γ conduction bands. The present data suggest that there is a Γ conduction band near 10.2 eV in CdSe.

In Table II we summarize features of the structure observed in the CdSe photoemission data and correlate the photoemission structure with optical data.

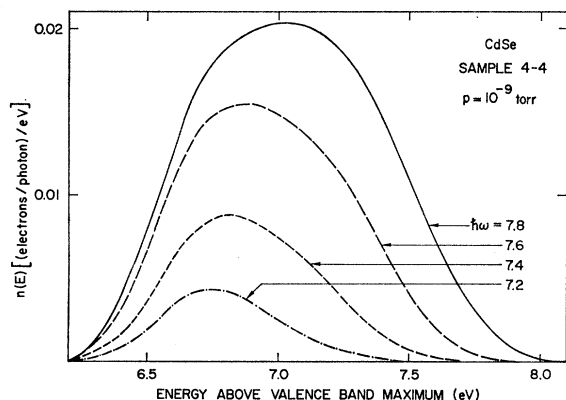


FIG. 11. Normalized energy distributions of the photoemitted electrons for the high-vacuum-cleaved crystal. $7.2 \leq \hbar\omega \leq 7.8$ eV.

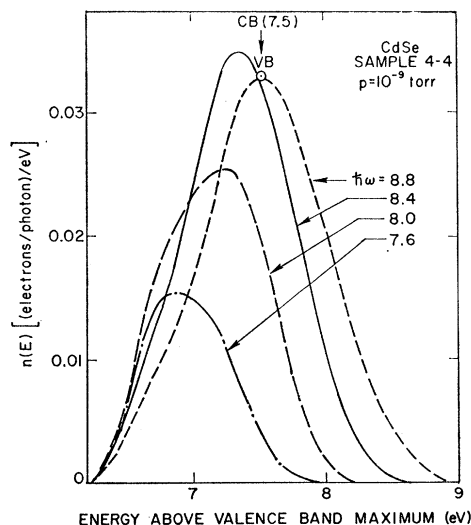


FIG. 12. Normalized energy distributions of the photoemitted electrons for the high-vacuum-cleaved crystal. $7.6 \leq \hbar\omega \leq 8.8$ eV.

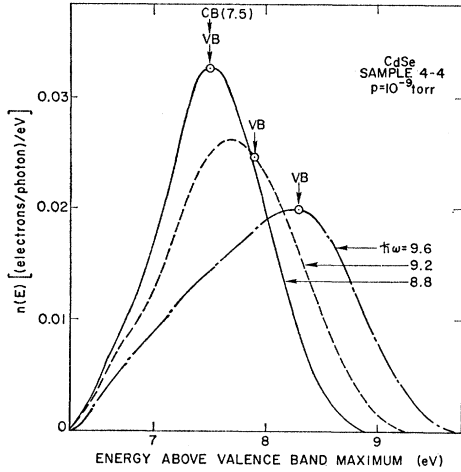


FIG. 13. Normalized energy distributions of the photoemitted electrons for the high-vacuum-cleaved crystal. $8.8 \leq \hbar\omega \leq 9.6$ eV.

C. Density-of-States Analysis of CdSe Photoemission Data

The qualitative discussion in the previous section indicated that the photoemission from CdSe results from a mixture of nondirect and matrix-element-dependent transitions. In this section we use the density-of-states analysis to (1) explicitly demonstrate the simultaneous presence of both types of transitions, and to (2) separate the effects of the nondirect transitions from those of the matrix-element-dependent transitions. The details of this analysis and an example of its application have been given elsewhere.² In Sec. IV D we show that the pseudopotential band structure suggests that most of the observed matrix-element-dependent transitions are due to direct transitions.

1. High-Vacuum Data

In Figs. 15 and 16 we present the valence-band optical densities of states and conduction-band effective optical

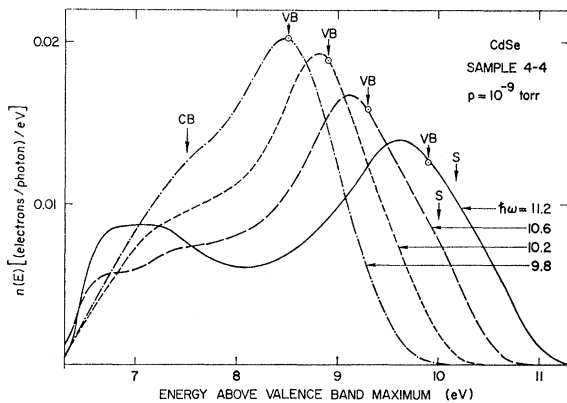


FIG. 14. Normalized energy distributions of the photoemitted electrons for the high-vacuum-cleaved crystal. $9.8 \leq \hbar\omega \leq 11.2$ eV. The structure below 7 eV for $\hbar\omega = 10.6$ and 11.2 eV is due to photoemission from the collector which we have not subtracted out of the raw data.

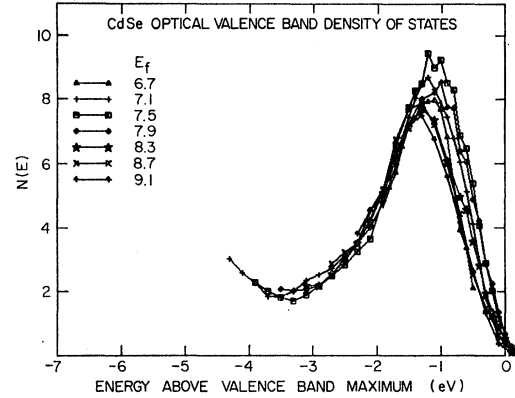


FIG. 15. CdSe valence-band ODS determined by density-of-states analysis of high-vacuum photoemission data (sample 4-4). E_f is the conduction-band energy used to derive the valence-band ODS.

densities of states (EODS) derived using the data for the sample cleaved at a pressure of 10^{-9} Torr. E_f is the energy of the final state used to derive the valence-band ODS, and E_i is the energy of the initial state used to derive the conduction EODS. Recall that if the valence-band ODS's seen by various final energies superimpose and the conduction band EODS's seen by various initial energies superimpose, then one must conclude that the nondirect model is sufficient to explain the photoemission data. The extent to which the densities of states do not superimpose indicates the relative strength of direct transitions.

Except for $E_i = -0.7$ and -1.1 eV in Fig. 16, the nondirect model provides a satisfactory explanation for most of the photoemission from the high-vacuum-cleaved sample. The optical density of states for the nondirect transitions (Fig. 17) is taken as an average of the curves in Figs. 15 and 16. The apparent rise in the valence-band ODS (Figs. 15 and 17) for $E_f \leq -3.3$ eV is due to the appearance of secondary electrons in

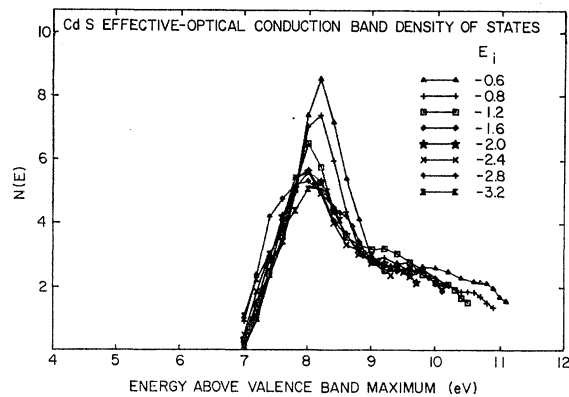


FIG. 16. CdS conduction-band EODS determined by density-of-states analysis of high-vacuum photoemission data (sample 4-4). E_i is the valence-band energy used to derive the conduction-band EODS. The failure of these curves to superimpose is due to direct transitions.

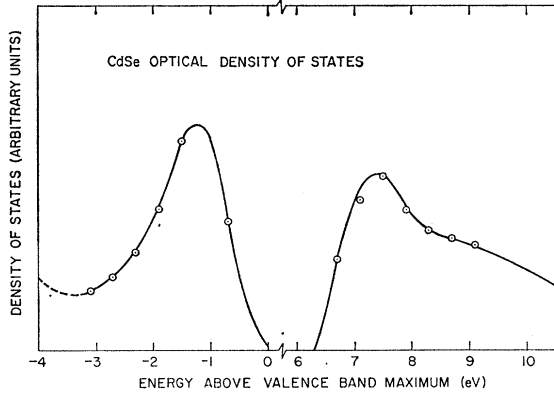


FIG. 17. CdSe optical density of states for nondirect transitions. This curve is an average of Figs. 15 and 16. The points indicate the values of the density of states used in deriving the results in Figs. 15 and 16. The conduction-band EODS involves the threshold function (surface-transmission probability) and the inelastic-scattering probability in addition to the conduction-band ODS. The dashed curve below about -3 eV in the valence-band ODS is due to the appearance of inelastically scattered electrons in the energy distributions. The amplitude of the valence-band ODS relative to the conduction-band EODS is not determined by our data.

the NEDC. Ignoring this rise, this analysis shows that the valence band ODS peaks near -1.3 eV and is about 3.3 eV wide.

Since the conduction-band EODS is determined directly from the photoemission NEDC, it involves the threshold function and inelastic-scattering probability in addition to the conduction-band ODS (Sec. II). The rapid rise in the conduction-band EODS (Fig. 17) for $6.3 < E < 7.1$ eV is due to the surface-transmission probability (threshold function) which goes to zero for $E \leq 6.3$ eV and rises rapidly for $E > 6.3$ eV. The decrease in the conduction-band EODS for $E \gtrsim 8$ eV indicates that the probability of inelastic scattering increases with increasing electron energy.

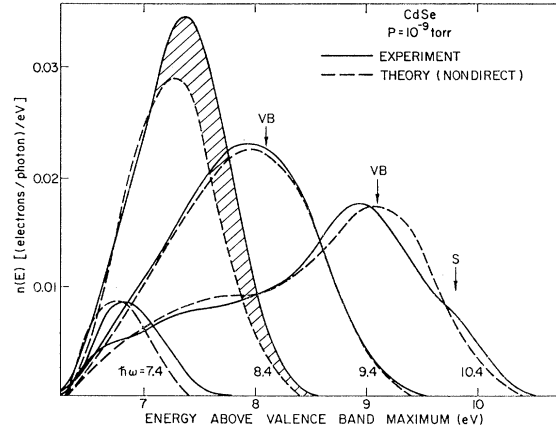


FIG. 18. Comparison of normalized energy distributions predicted by nondirect theory and experiment. Theoretical curves result from Eq. (2) and the optical density of states shown in Fig. 17. The shaded portion of the experimental curve for $\hbar\omega = 8.4$ eV is due to direct transitions.

We demonstrate explicitly the relative importance of direct and nondirect transitions by choosing an average optical density of states from Figs. 15 and 16 and calculating the nondirect contribution to the NEDC using

$$n(E, \hbar\omega) = N_c(E)N_v(E - \hbar\omega), \quad (2)$$

where $n(E, \hbar\omega)$ is the density of photoemitted electrons at energy E above the top of the valence band for a photon energy $\hbar\omega$, $N_c(E)$ is the conduction-band EODS at E , and $N_v(E - \hbar\omega)$ is the valence-band ODS at $E - \hbar\omega$. Using the optical density of states shown in Fig. 17, we calculate the NEDC shown in Fig. 18. The experimental curves have been normalized to the yield, but the calculated curves are identically the result of Eq. (2).

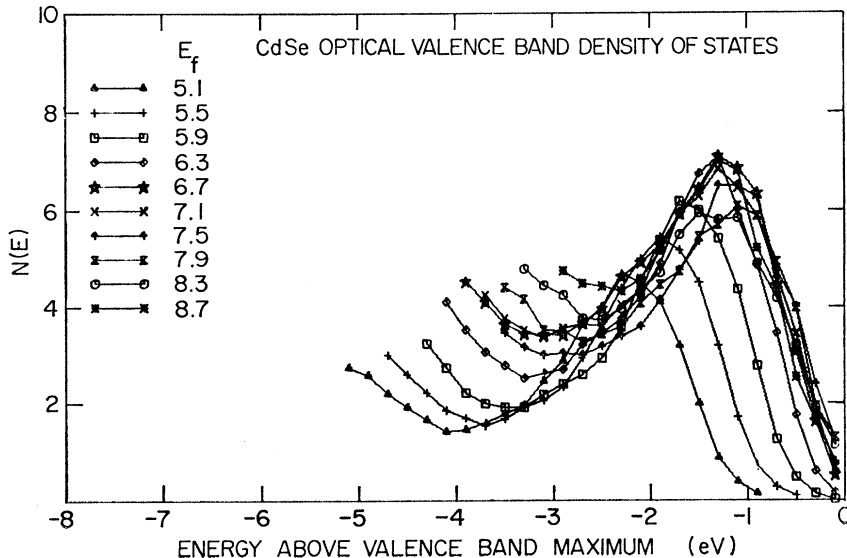
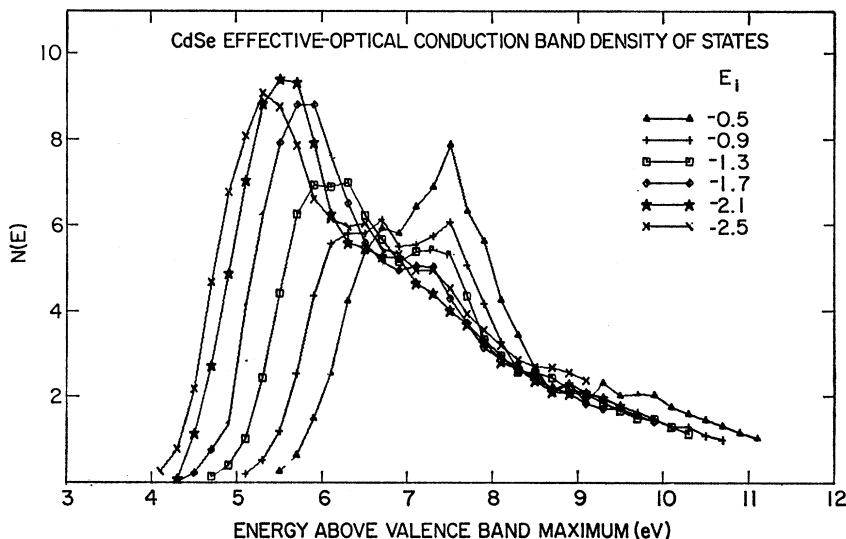


FIG. 19. CdSe valence-band ODS determined by density-of-states analysis of low-vacuum photoemission data (sample 4-3). E_f is the conduction-band energy used to derive the valence-band ODS.

FIG. 20. CdSe conduction-band EODS determined by density-of-states analysis of low-vacuum photoemission data (sample 4-3). E_i is the valence-band energy used to derive the conduction-band EODS. The failure of the curves to superimpose is due to direct transitions.



The principal results of the high-vacuum study of the photoemission from CdSe are summarized in Fig. 18. Most of the photoemission is due to nondirect transitions. Peak VB moves in accordance with Eq. (1), indicating that conservation of wave vector is not an important selection rule for these transitions, and, for $\hbar\omega > 8.8$ eV, peak CB remains at 7.5 eV due to nondirect transitions to a peak in the conduction-band density of states. The difference between nondirect theory and experiment for $\hbar\omega = 8.4$ eV (Fig. 18) is due to direct transitions. Although these direct transitions (shaded in Fig. 18) account for only 20% of the total photoemission at $\hbar\omega = 8.4$ eV, the number of electrons excited to some energies near 8 eV is twice as much as predicted by the nondirect model. The presence of these direct transitions for $\hbar\omega \approx 8.4$ eV explains why the

optical data and NEDC have maxima for $\hbar\omega = 8.4$ eV even though the nondirect transitions are strongest for $\hbar\omega = 8.8$ eV when the valence-band peak at -1.3 eV is coupled to the conduction-band peak at 7.5 eV. We have indicated in Fig. 10 our estimate of the contribution of direct transitions to $\epsilon_2\omega^2$.

We mentioned in Sec. IV B that the high-energy shoulder S appeared to be due to direct transitions to conduction-band states near 10.2 eV. This is also clear in Fig. 18 for $\hbar\omega = 10.4$ eV. The direct transitions causing the shoulder S appear in addition to the nondirect transitions. The reason why VB in the experimental NEDC is shifted slightly to lower energy for $\hbar\omega = 10.4$ eV is not understood.

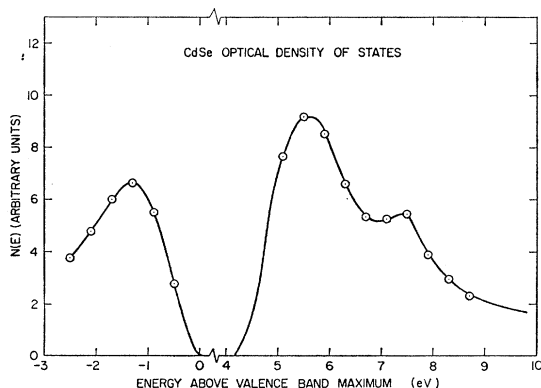


FIG. 21. CdSe optical density of states used to derive the strength of coupling shown in Fig. 22. The points indicate the values of the density of states used in deriving the results in Figs. 19 and 20. The conduction-band EODS involves the threshold function (surface-transmission probability) and the inelastic-scattering probability in addition to the conduction-band ODS. The amplitude of the valence-band ODS relative to the conduction-band EODS is not determined by our data.

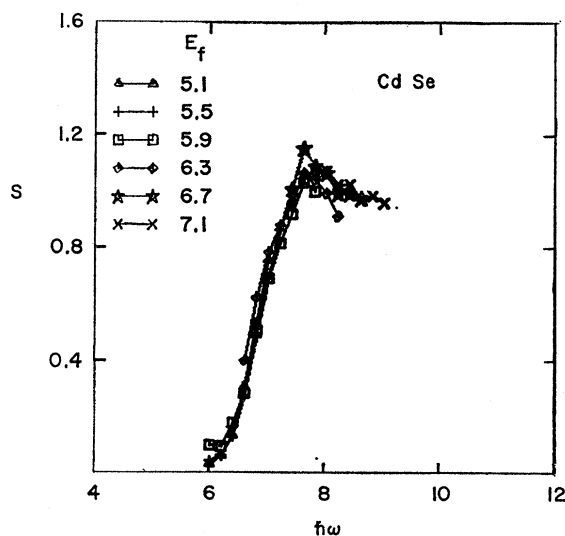


FIG. 22. The strength of coupling to a final state E_f for a photon energy $\hbar\omega$. The optical density of states in Fig. 21, together with the experimental energy distributions, was used in Eq. (3) to derive these results.

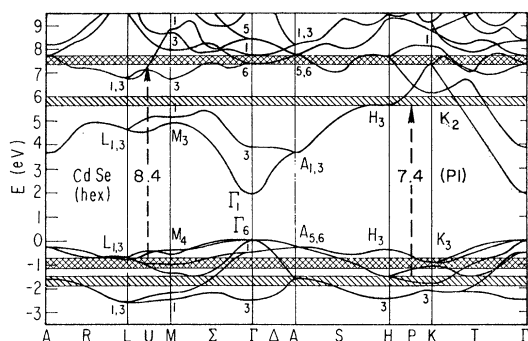


FIG. 23. Pseudopotential band structure for wurtzite CdSe (Ref. 16). The shaded sections separated by 7.4 eV are the initial and final states responsible for the direct transitions ($P1$) observed in the energy distributions for $\hbar\omega \approx 7.4$ eV. The shaded sections separated by 8.4 eV are the initial and final states responsible for the weak direct transitions observed in the energy distributions for $\hbar\omega \approx 8.4$ eV.

2. Low-Vacuum Data

We have also performed the density-of-states analysis on the photoemission data for the sample cleaved in the monochromator vacuum, and the results are shown in Figs. 19 and 20. As shown in Secs. IV B and VI, effects of the poorer vacuum are (1) lowering of the electron affinity by more than one volt, and (2) the appearance of a large number of secondary electrons in the EDC. This latter effect has a large influence on the derived

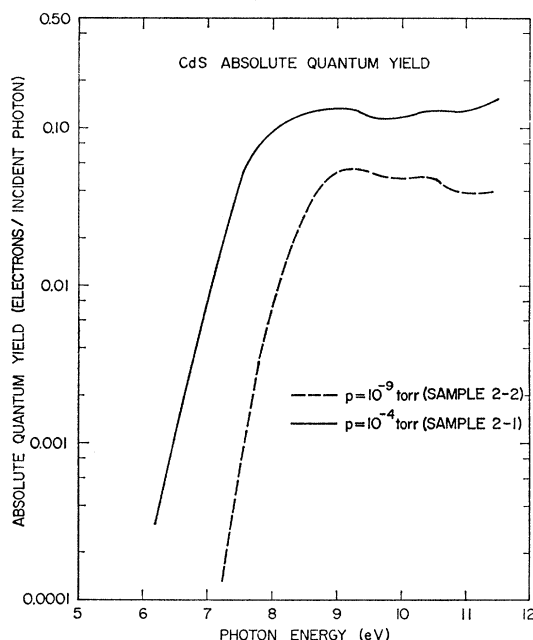


FIG. 24. Absolute quantum yields for a crystal of CdS cleaved in high vacuum (pressure = 10^{-9} Torr) and in low vacuum (pressure = 10^{-4} Torr). The pressure of 10^{-4} Torr consists of hydrogen and a 10^{-7} Torr background pressure of the oil-diffusion pump. In another experiment (described in the text) we show that the reduced electron affinity in the low-vacuum experiment is entirely due to the background pressure of 10^{-7} Torr.

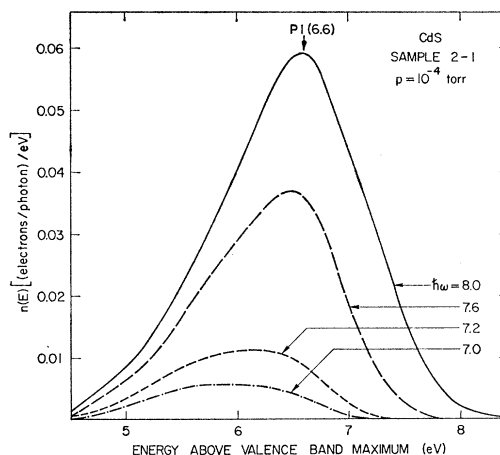


FIG. 25. Normalized energy distributions of the photoemitted electrons for the low-vacuum-cleaved crystal. $7.0 \leq \hbar\omega \leq 8.0$ eV.

valence-band ODS below about -2.2 eV. Comparing the valence-band ODS for the high-vacuum data (Fig. 15) and for the low-vacuum data (Fig. 19), we find that for $E \lesssim 2.2$ eV there is a large apparent valence-band density of states for the low-vacuum data that is not present in the high-vacuum data. This difference is due to the appearance of scattered electrons in the NEDC. For more details of the effects of electron-electron scattering see Sec. VI.

For conduction-band states observable in both high- and low-vacuum experiments, the results of this analysis agree with the analysis of the high-vacuum data in Sec. IV C 1 and will not be discussed further. On the other hand, the lower electron affinity for the low-vacuum-cleaved sample allows us to observe strong structure in the photoemission due to final states which lie below the vacuum level in the high-vacuum experiments.

We see in Figs. 19 and 20 that for final states between about 4.5 and 6.5 eV, the nondirect model is completely inadequate to explain the photoemission data. Matrix elements are indeed important. The transition probability coupling initial states close to the top of the valence band to final states in the region $4.5 \lesssim E_f \lesssim 6.5$ eV is much weaker than that coupling deeper valence-band states to these same final states. This variation in the strength of coupling is not due to the variation in the density of states since the valence-band ODS is factored out when the curves in Fig. 20 are derived from the NEDC.^{2,9,10,13} Of course, for $-1.8 < E_i < 0$ these differences among the curves in Fig. 20 cannot be due to the appearance of secondary electrons in the NEDC. These curves actually plot the relative number of electrons photoemitted at an energy $-E_i$ below the highest-energy electron, and the minimum energy loss through electron-electron scattering is equal to the band gap of 1.8 eV.

It is apparent in Fig. 20 that the details of the photoemission from conduction-band states in the region

$4.5 \lesssim E \lesssim 6.5$ eV are very complicated. Nonetheless, we show in Sec. IV D that the pseudopotential band calculation¹⁶ for CdSe provides a qualitative explanation for the appearance of this structure in the NEDC. The basic idea is that the conduction-band density of states is weak in the region $4.5 \lesssim E \lesssim 6.5$ eV; hence there are few nondirect transitions to these states. Then when the photon energy is just right for direct transitions to take place to these final states, it results in a large increase in the number of photoemitted electrons.

From the photoemission data we are able to deduce a line shape for the onset of these direct transitions to final states in the region $4.5 \lesssim E_f \lesssim 6.5$ eV. The possible significance of this line shape will be discussed below. Let us define $S(E_f, \hbar\omega)$, the *strength of coupling* to a final state at energy E_f for a photon energy $\hbar\omega$, by the relation

$$n(E_f, \hbar\omega) = S(E_f, \hbar\omega) N_c(E_f) N_v(E_f - \hbar\omega). \quad (3)$$

The quantities N_c , N_v , and n were defined following Eq. (2). If the nondirect model were sufficient to explain the photoemission data, then $S(E_f, \hbar\omega)$ would equal a constant for all E_f and $\hbar\omega$. When the nondirect model is not sufficient, then in general the function S for one final energy will not be simply related to that for another final energy.

Obviously, there is a considerable amount of arbitrariness in the choice of N_c , N_v , and S . For any arbitrary N_c and N_v , a set of S 's can be constructed so that Eq. (3) reproduces the experimental NEDC. However, the feature we wish to point out here is that for one particular choice of N_c and N_v , S has a very simple form. If in Eq. (3) we use the optical density of states shown in Fig. 21 and the NEDC presented earlier, we derive the strength of coupling shown in Fig. 22. The striking feature about Fig. 22 is that for $E_f \lesssim 7.2$ eV, the strength of coupling is a function of $\hbar\omega$ only and rises by a factor of 20 between $\hbar\omega = 6.0$ and

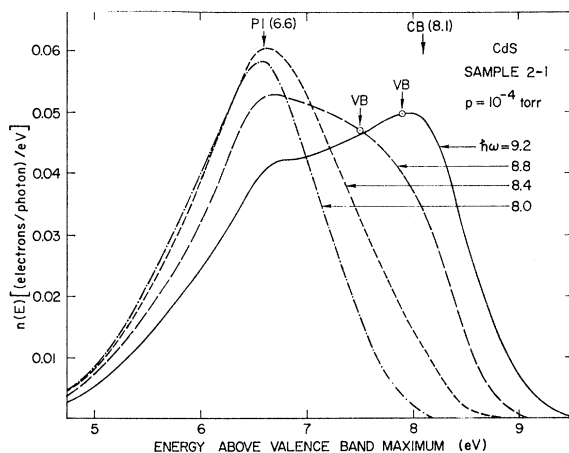


FIG. 26. Normalized energy distributions of the photoemitted electrons for the low-vacuum-cleaved crystal. $8.0 \leq \hbar\omega \leq 9.2$ eV.

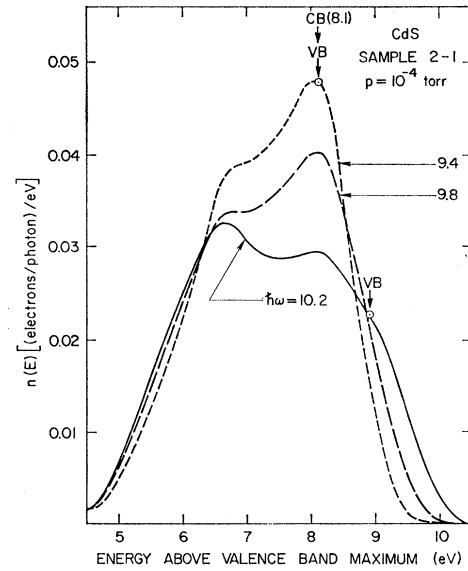


FIG. 27. Normalized energy distributions of the photoemitted electrons for the low-vacuum-cleaved crystal. $9.4 \leq \hbar\omega \leq 10.2$ eV.

7.2 eV. The nondirect model fails by as much as a factor of 20 in the region $6.0 < \hbar\omega < 7.2$ eV. This rise in the strength of coupling for $6.0 < \hbar\omega < 7.2$ eV accounts for the rapid rise in $\epsilon_2\omega^2$ (Fig. 10) for the same photon energies.

It is remarkable that one needs only two curves to generate the NEDC for energies below about 7.0 eV for any photon energy. These are: (1) the optical density of states shown in Fig. 21, and (2) the strength of coupling shown in Fig. 22. Nonetheless, there may be no significance to this particular decomposition of the NEDC. As remarked earlier, for any arbitrary choice of N_c and N_v in Eq. (3), a set of S 's can be constructed so that Eq. (3) reproduces the experimental NEDC.

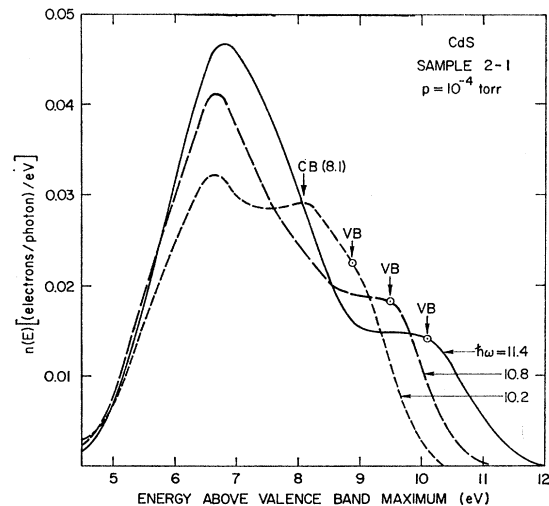


FIG. 28. Normalized energy distributions of the photoemitted electrons for the low-vacuum-cleaved crystal. $10.2 \leq \hbar\omega \leq 11.4$ eV.

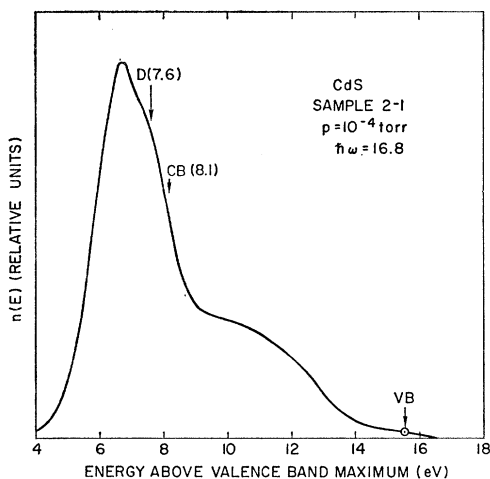


FIG. 29. Energy distribution of the photoemitted electrons for the low-vacuum-cleaved crystal. $\hbar\omega = 16.8$ eV.

There are two points which suggest that the strength of coupling shown in Fig. 22 is physically significant. The first point is that we show in Sec. V C that a similar result explains the photoemission from CdS (see Fig. 44). Secondly, in both cases the shapes of the strength of coupling explain the rapid rises in $\epsilon_2\omega^2$. Further theoretical work is necessary before the physical significance of Fig. 22 can be verified. In any attempt to make a quantitative comparison of the optical density of states (Fig. 21) with theory, it must be remembered that the conduction-band EODS involves the threshold function (surface-transmission probability) and inelastic-scattering probability as well as the true conduction-band optical density of states. For example, if the escape depth is a rapidly decreasing function of electron energy, then the conduction-band ODS may actually increase between 5.5 and 7.5 eV although the effective density of states decreases in this region (Fig. 21).

D. Band Structure of CdSe

We have shown earlier that both direct and nondirect transitions contribute to the photoemission from CdSe.

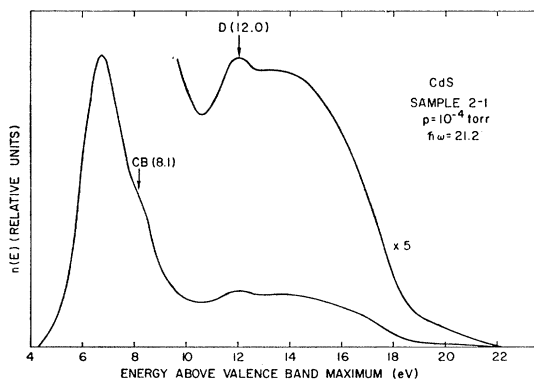


FIG. 30. Energy distribution of the photoemitted electrons for the low-vacuum-cleaved crystal. $\hbar\omega = 21.2$ eV.

In this section we discuss the assignment of the direct transitions to specific regions of the Brillouin zone.

Usually one must perform volume integrals over the Brillouin zone to definitively assign structure in the joint density of states (i.e., one must calculate $\epsilon_2\omega^2$). However, this is not the case for the strong structure observed in both photoemission and optical properties of CdSe near a photon energy of 7.4 eV. We showed in Sec. IV C that this structure resulted from the rapid rise in the strength of coupling between initial and final states (see Figs. 19–22). As summarized in Table II, the photoemission data determine that the initial states for this transition are centered near -1.6 eV and the final states are near 5.8 eV. We have sketched these states onto Bergstresser and Cohen's¹⁶ pseudopotential band structure presented in Fig. 23. It is immediately apparent that the most important states contributing to the structure at a photon energy of 7.4 eV lie near the zone edge connecting H and K . Figure 23 indicates that there are very few 5.8-eV conduction-band states

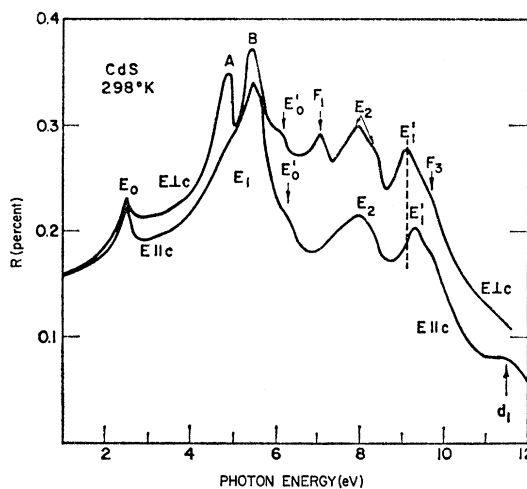


FIG. 31. Reflectivity of CdS measured by Cardona and Harbeke (Ref. 17).

anywhere in the zone other than near this zone edge. Hence there is a small density of states at 5.8 eV; and as a result, there are very few nondirect transitions to 5.8 eV. When direct transitions can take place to these final states, it is a large effect as is observed in the photoemission data (Fig. 20).

We have also sketched onto Fig. 23 the states which caused the NEDC and $\epsilon_2\omega^2$ to peak for $\hbar\omega = 8.4$ eV. It is not clear which regions of the Brillouin zone are producing this structure. Bergstresser and Cohen¹⁶ have assigned this structure to $\Gamma_5 \rightarrow \Gamma_6$ and $\Gamma_1 \rightarrow \Gamma_1$ transitions. It appears that the initial states lie too deep for this assignment to be the most important contribution to the observed structure. We showed in Sec. IV C that for $\hbar\omega = 8.4$ eV, the direct transitions accounted for only 20% of the photoemission, the remaining 80% being due to nondirect transitions. This is understandable

since Fig. 23 shows that there are conduction-band states near 7.5 eV over a large region of the zone.

V. PHOTOEMISSION STUDY OF CdS

Kindig and Spicer⁵ (hereafter referred to as KS) have previously studied the photoemission from vacuum-cleaved single crystals of CdS and found that the qualitative features were due to nondirect transitions. Using the density of states deduced from the photoemission data, KS then calculated a theoretical absorption spectrum, assuming nondirect transitions and constant matrix elements. This theoretical spectrum²² reproduced the gross features of the experimental curve determined by Walker and Osantowski. However, the nondirect calculation did not predict the sharp peaks of the experimental absorption spectrum.

We undertook the present study of CdS in an attempt to explain the portions of the absorption spectrum which were not due to nondirect transitions. We have re-measured both the NEDC and the quantum yield. The shapes of the NEDC presented here are indistinguishable from those of KS⁵; however, because of an

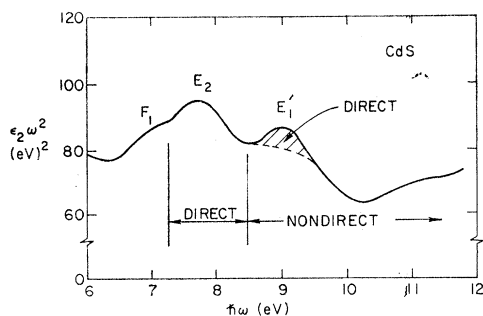


FIG. 32. The imaginary part of the dielectric function (ϵ_2) times the square of the photon energy. We evaluated this function using optical data obtained by Cardona and Harbeke (Ref. 17) from a Kramers-Kronig transform of their reflectance data. We indicate on this figure our estimate of the contributions of direct and nondirect transitions.

improved calibration of reference standards,¹⁵ our yield curves differ from those measured by KS⁵ by as much as a factor of 2 in some regions. The estimated uncertainty in the present yield is $\pm 10\%$.

Through the detailed analysis presented in Sec. V C, we find that, in fact, direct transitions appear in the NEDC for the photon energies of the peaks in the absorption spectrum. In Sec. V C we show that the pseudopotential band structure for CdS calculated by Bergstresser and Cohen¹⁶ locates the important region of the Brillouin zone for one of these peaks although the origin of the other is less certain.

The features of the NEDC from CdS are remarkably similar to those from CdSe except that the relevant

²² See Fig. 19 of Ref. 5. Note, however, that this figure contains a misprint: The legends for the calculated curves should be interchanged.

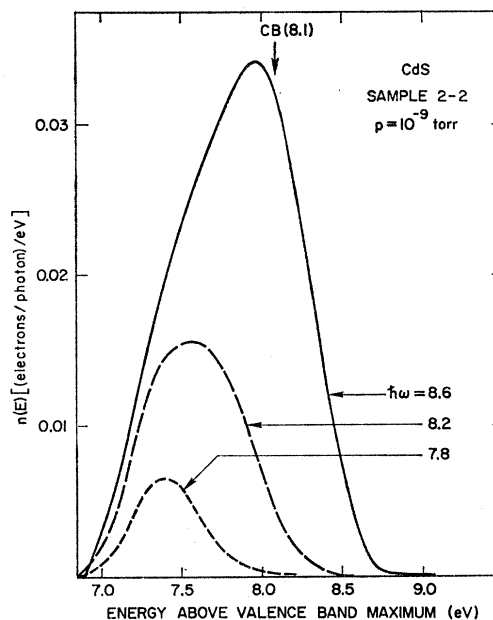


FIG. 33. Normalized energy distributions of the photoemitted electrons for the high-vacuum-cleaved crystal. $7.8 \leq h\omega \leq 8.6$ eV.

conduction-band structure lies ~ 0.5 eV higher in CdS than in CdSe. In fact, there is a one-to-one correspondence between structure in the CdS and CdSe NEDC. The sole exception is the weak structure DT in CdSe (Figs. 4 and 5) which is not observed in CdS. Because of this similarity of the CdSe and CdS data, we do not repeat here a detailed discussion of the structure in the CdS NEDC. Rather, we merely present the revised absolute yield, the normalized energy distributions, and summarize the important results in Table III.

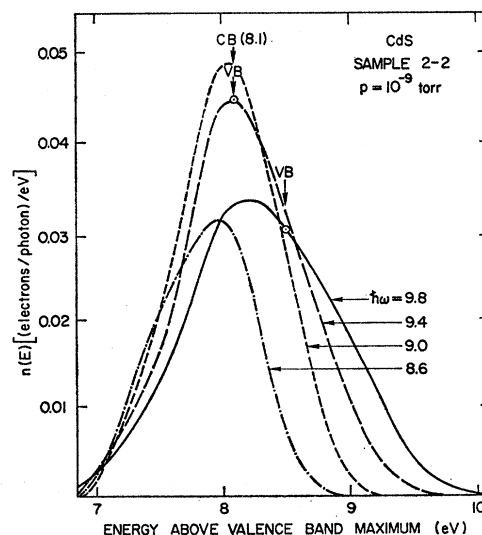


FIG. 34. Normalized energy distributions of the photoemitted electrons for the high-vacuum-cleaved crystal. $8.6 \leq h\omega \leq 9.8$ eV.

TABLE III. Correlation of photoemission and optical data for CdS.

$\hbar\omega$ (eV)	Energy of final state ^c	Photoemission data ^a		Assignment suggested by this work	Reflectivity data ^b	
		Energy of initial state ^c	Nature of transition		$\hbar\omega$ (eV)	Label
8.0	6.6 (P1)	-1.4	Direct	Near zone edge connecting <i>H</i> & <i>K</i>	8.2 (7.8)	E_2
9.0	~8.1	~-0.9	Direct	Unknown	9.25 (9.0)	E_1'
9.4	8.1 (CB)	-1.3 (VB)	Nondirect	Peaks in density of states	9.8	F_3
$\gtrsim 8.8$	$\hbar\omega - 1.3$	-1.3 (VB)	Nondirect	Peak in valence-band density of states
$\gtrsim 8.1$	8.1	...	Nondirect	Peak in conduction-band density of states
...	...	-9.2 (D)	(Nondirect)	Transitions from <i>d</i> band	14	d_2
>10.6	10.6 (S)	~-0.0	Direct	Near Γ	11.5	d_1

^a Labels in parentheses refer to structure in Figs. 25-30, and 33-36.

^b Reflectivity data (Fig. 31) are taken from Ref. 17. Numbers in parentheses are taken from the $\epsilon_2\omega^2$ plot in Fig. 32.

^c Energies are given in electron volts above the valence-band maximum. The estimated uncertainty in the location of peaks in the NEDC is ± 0.2 eV.

A. Quantum Yield

We present in Fig. 24 the absolute quantum yield for a crystal of CdS cleaved in ultrahigh vacuum and for the same crystal cleaved in low vacuum. The electron affinity for the low-vacuum-cleaved sample is more than a volt lower than for the high-vacuum-cleaved sample and the low-vacuum yield is everywhere greater than the high-vacuum yield.

B. Energy Distributions of the Photoemitted Electrons

In Figs. 25-30 we present normalized energy distribution curves (NEDC) for a crystal cleaved in the vacuum of the monochromator (see Sec. III). Except for $\hbar\omega = 16.8$ and 21.2 eV, all curves have been normalized to the quantum yield. In Fig. 31, the reflectivity of Cardona and Harbeke (Ref. 17) for light, polarized perpendicular and parallel to the *C* axis, is presented. The $\epsilon_2\omega^2$ obtained by the present workers from the data of Cardona and Harbeke using a Kramers-Kronig transform of their reflectance data is given in Fig. 32.

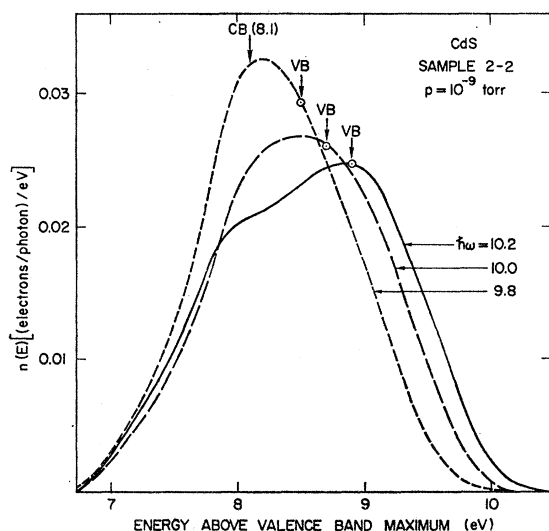


FIG. 35. Normalized energy distributions of the photoemitted electrons for the high-vacuum-cleaved crystal. $9.8 \leq \hbar\omega \leq 10.2$ eV.

In Figs. 33-36 we present NEDC for the same crystal cleaved in a vacuum of 10^{-9} Torr.

C. Density-of-States Analysis of CdS Photoemission Data

The photoemission from CdS results from mixture of nondirect and matrix-element-dependence transitions. In this section we use the density-of-states analysis to (1) explicitly demonstrate the simultaneous presence of both types of transitions, and to (2) separate the effects of the nondirect transitions from those of the matrix-element-dependent transitions. The details of this analysis and an example of its application have been given elsewhere.² In Sec. V D we show that the CdS pseudopotential band structure¹⁶ suggests that most of the observed matrix-element-dependent transitions are due to direct transitions.

1. High-Vacuum Data

In Figs. 37 and 38 we present the valence-band ODS and conduction-band EODS derived using the data for

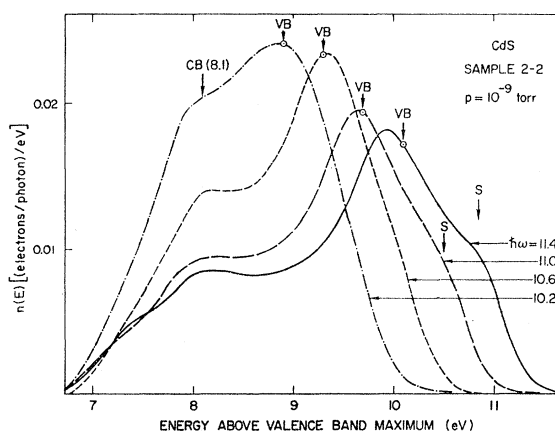


FIG. 36. Normalized energy distributions of the photoemitted electrons for the high-vacuum-cleaved crystal. $10.2 \text{ eV} \leq \hbar\omega \leq 11.4$ eV. The small shoulder near 7.3 eV for $\hbar\omega = 11.4$ eV is due to the appearance of a small amount of reverse current (photoemission from the collector due to reflected light).

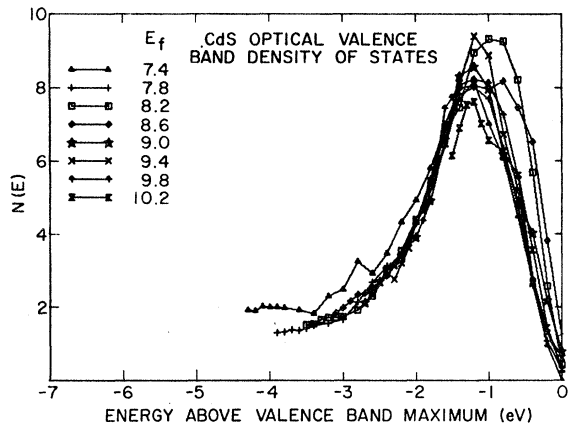


FIG. 37. CdS valence-band optical density of states determined by density-of-states analysis of high-vacuum photoemission data (sample 2-2). E_f is the conduction-band energy used to derive the valence-band ODS.

the sample cleaved at a pressure of 10^{-9} Torr. Except for $E_i = -0.6$ and -0.8 eV in Fig. 38, the nondirect model provides a satisfactory explanation for most of the photoemission from the high-vacuum-cleaved sample. The optical density of states for the nondirect transitions (Fig. 39) is taken as an average of the curves in Figs. 37 and 38. The apparent rise in the ODS (Figs. 37 and 39) for $E \leq -3.0$ eV is due to the appearance of secondary electrons in the NEDC. Ignoring this rise, this analysis shows that the valence-band ODS peaks near -1.3 eV and is about 3.0 eV wide.

Following the analysis of the CdSe data in Sec. IV C, we demonstrate explicitly the relative importance of direct and nondirect transitions by choosing an average ODS from Figs. 37 and 38 and calculating the nondirect contribution to the NEDC using Eq. (2). Using the ODS shown in Fig. 39, we calculate the NEDC shown in Fig. 40. The experimental curves have been normalized to yield, but the calculated curves are identically the result of Eq. (2).

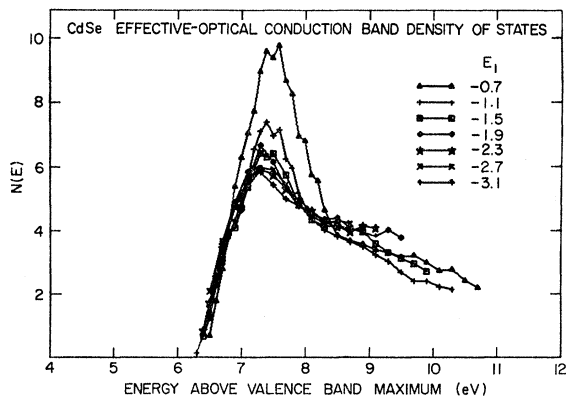


FIG. 38. CdS conduction-band effective optical density of states determined by density-of-states analysis of high-vacuum photoemission data (sample 2-2). E_i is the valence-band energy used to derive the conduction-band EODS. Failure of these curves to superimpose is due to direct transitions.

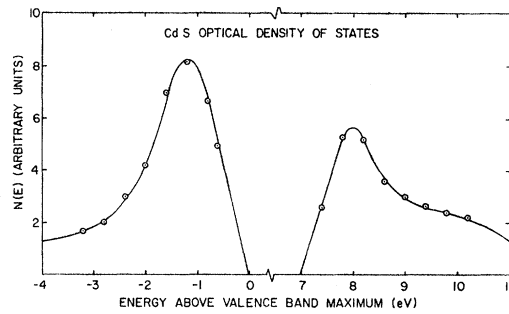


FIG. 39. CdS optical density of states for nondirect transitions. This curve is an average of Figs. 37 and 38. The points indicate the values of the optical density of states used in deriving the results in Figs. 37 and 38. The amplitude of the valence-band ODS relative to the conduction-band EODS is not determined by our data.

The principal results of the high-vacuum study of the photoemission from CdS are summarized in Fig. 40. Most of the photoemission is due to nondirect transitions. Peak VB moves in accordance with Eq. (3), indicating that conservation of wave vector is not an important selection rule for these transitions, and for $\hbar\omega > 9.4$ eV peak CB remains at 8.1 eV due to nondirect transitions to a peak in the conduction-band density of states. The difference between nondirect theory and experiment for $\hbar\omega = 9.0$ eV (Fig. 40) is due to direct transitions. Although these direct transitions (shaded in Fig. 40) account for only 20% of the total photoemission at $\hbar\omega = 9.0$ eV, the number of electrons excited to some energies near 8.5 eV is twice as much as predicted by the nondirect model. The presence of these direct transitions for $\hbar\omega \approx 9.0$ eV explains why the optical data and NEDC have maxima for $\hbar\omega = 9.0$ eV even though the nondirect transitions are strongest for $\hbar\omega = 9.4$ eV. We have introduced in Fig. 32 our estimate of the contribution of direct transitions to $\epsilon_2\omega^2$.

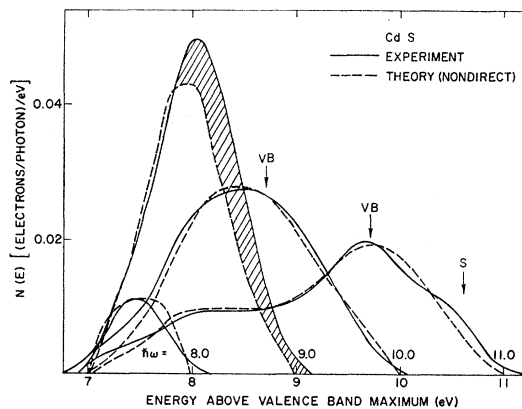


FIG. 40. Comparison of normalized energy distributions predicted by nondirect theory and experiment. Theoretical curves result from Eq. (2) and the optical density of states in Fig. 39. The shaded section in the experimental curve for $\hbar\omega = 9.0$ eV is due to direct transitions.

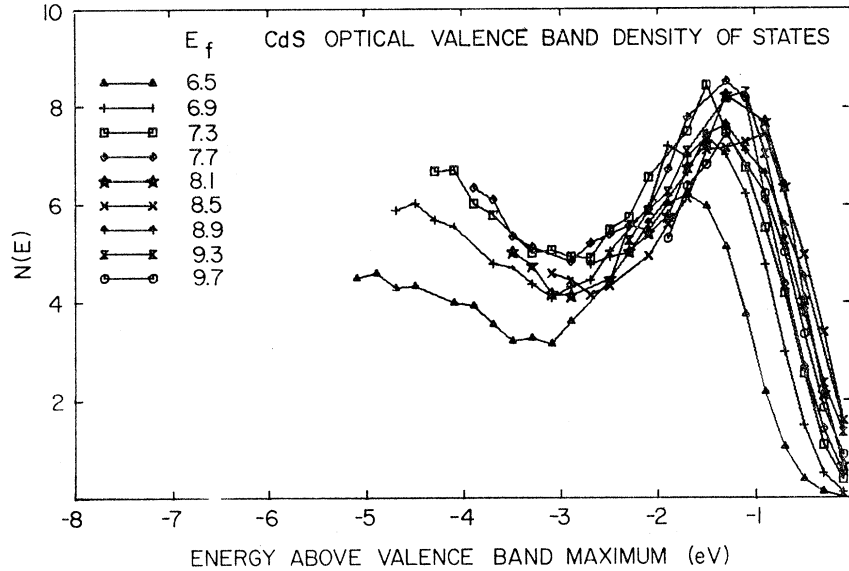


FIG. 41. CdS valence-band optical density of states determined by density-of-states analysis of low-vacuum photoemission data (sample 2-1). E_f is the conduction-band energy used to derive the valence-band ODS.

2. Low-Vacuum Data

We have also performed the density-of-states analysis on the photoemission data for the sample cleaved in the monochromator vacuum, and the results are shown in Figs. 41 and 42. For conduction-band states exposed in both high- and low-vacuum experiments, the results of this analysis agree with the analysis of the high-vacuum data in Sec. V C 1 and will not be discussed further. On the other hand, the lower electron affinity for the low-vacuum-cleaved sample allows us to observe strong structure in the photoemission from final states which lie below the vacuum level in the high-vacuum experiments.

We see in Figs. 41 and 42 that for final states between about 5.5 and 7.5 eV, the nondirect model is completely inadequate to explain the photoemission data. Matrix elements are indeed important. The transition probability coupling initial states close to the top of the valence band to final states in the region $5.5 \leq E_f \leq 7.5$ eV is much weaker than that coupling deeper valence-band states to these same final states.

It is apparent in Fig. 42 that the details of the photoemission from conduction-band states in the region $5.5 \leq E \leq 7.5$ eV are very complicated. Nonetheless, we show in Sec. V D that the pseudopotential band calculation¹⁶ for CdS provides a qualitative explanation

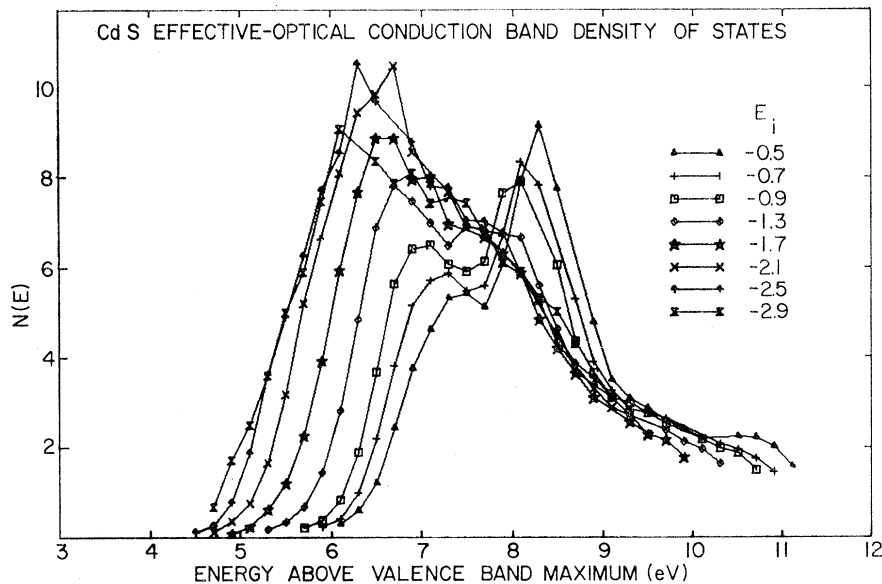


FIG. 42. CdS conduction-band effective optical density of states determined by density-of-states analysis of low-vacuum photoemission data (sample 2-1). E_i is the valence-band energy used to derive the EODS. Failure of these curves to superimpose is due to direct transitions.

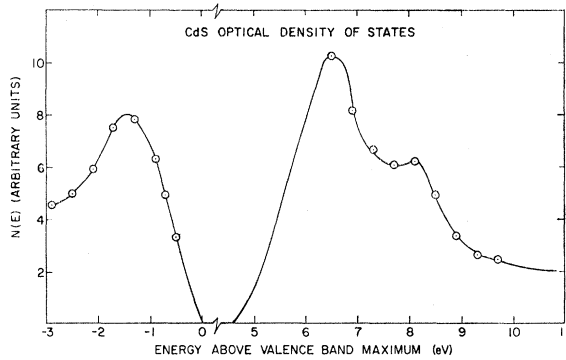


FIG. 43. CdS optical density of states used to derive the strength of coupling in Fig. 44. The points indicate the values of the optical density of states used in deriving the results in Figs. 41 and 42. The amplitude of the valence-band ODS relative to the conduction-band EODS is not determined by our data.

for the appearance of this structure in the NEDC. The basic idea is that the conduction-band density of states is weak in the region $5.5 \leq E \leq 7.5$ eV; hence there are few nondirect transitions to these states. Then when the photon energy is just right for direct transitions to take place to these final states, they result in a large increase in the number of photoemitted electrons.

In the discussion of the CdSe data in Sec. IV C, we showed that we are able to deduce from the photoemission data a line shape for the onset of these direct transitions to final states in the region $5.5 \leq E_f \leq 7.5$ eV. The strength of coupling $S(E_f, \hbar\omega)$ between initial and final states was defined by Eq. (3). Using the optical density of states shown in Fig. 43 and the NEDC presented earlier, we derive the strength of coupling shown in Fig. 44. The striking feature in Fig. 44 is that for $E_f \leq 8.5$ eV, the strength of coupling is approximately a function of $\hbar\omega$ only and rises by about a factor of 20 between $\hbar\omega = 6.8$ and 8.5 eV. Hence the nondirect model fails by as much as a factor of 20 in this region. This rise in the strength of coupling for $\hbar\omega > 6.8$ eV explains the rapid rise in $\epsilon_2\omega^2$ (Fig. 32) for the same photon energies.

D. Band Structure of CdS

We have shown earlier that both direct and nondirect transitions contribute to the photoemission from CdS. In this section we discuss the assignment of the direct transitions to specific regions of the Brillouin zone. We have sketched the initial and final states for these transitions onto Bergstresser and Cohen's¹⁶ pseudopotential band structure in Fig. 45. It is immediately apparent that the most important states contributing to the structure at a photon energy of 8.0 eV lie near the zone edge connecting H and K . Figure 45 indicates that there are very few 6.6 eV conduction-band states anywhere in the zone other than near this zone edge. Hence there is a very small density of states at 6.6 eV; and as a result, there are very few nondirect transi-

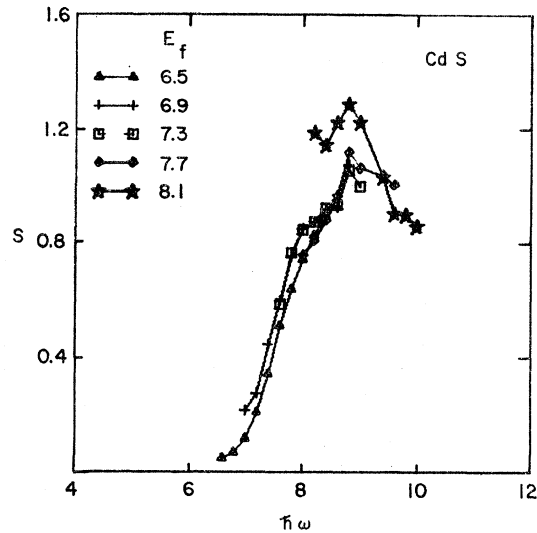


FIG. 44. The strength of coupling to a final state E_f for a photon energy $\hbar\omega$. The optical density of states in Fig. 43, together with the experimental energy distributions, was used in Eq. (3) to derive these results.

tions to 6.6 eV. When direct transitions can take place to these final states, it is as large an effect as is observed in the photoemission data (Fig. 42).

We have also sketched onto Fig. 45 the states which cause the NEDC and $\epsilon_2\omega^2$ to peak for $\hbar\omega = 9.0$ eV. It is not clear which regions of the Brillouin zone are producing this structure. Bergstresser and Cohen¹⁶ have assigned this structure to $\Gamma_5 \rightarrow \Gamma_6$ and $\Gamma_1 \rightarrow \Gamma_1$ transitions. It appears that the initial states lie too deep for this assignment to be the most important contribution to the observed structure. We showed in Sec. V C that for $\hbar\omega = 9.0$ eV, the direct transitions accounted for only 20% of the photoemission. This is understandable since Fig. 45 shows that there are conduction-band states near 6.6 eV over a large region of the zone.

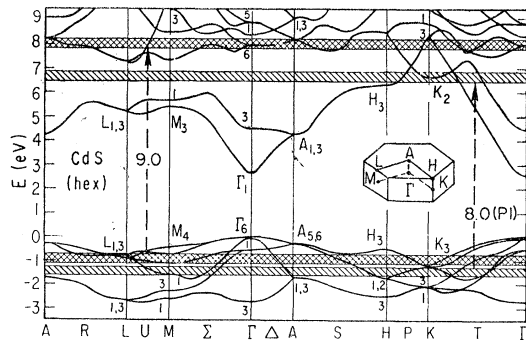


FIG. 45. Pseudopotential band structure for wurtzite CdS (Ref. 16). The shaded sections separated by 8.0 eV are the initial and final states responsible for the direct transitions observed in the energy distributions (P_1) for $\hbar\omega \approx 8.0$ eV. Similarly the shaded sections separated by 9.0 eV are the initial and final states responsible for the weak direct transitions observed in the energy distributions for $\hbar\omega \approx 9.0$ eV.

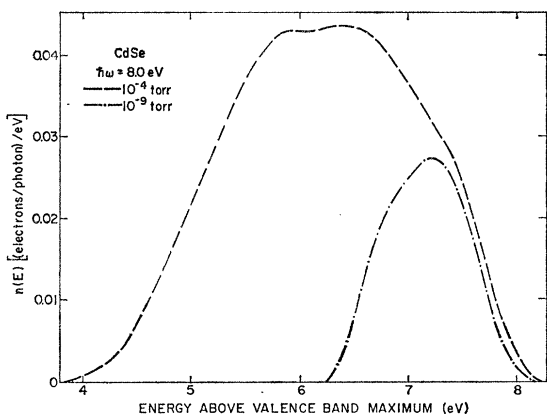


FIG. 46. Comparison of normalized energy distributions from the high-vacuum-cleaved and the low-vacuum-cleaved crystals for $\hbar\nu = 8.0$ eV.

VI. EFFECTS OF ELECTRON-ELECTRON SCATTERING

A. Energy Distribution Curves

Effects due to electron-electron scattering are observed in the photoemission data. The qualitative features of the scattering are similar in CdSe and CdS. To illustrate these effects, we discuss the scattering observed in the CdSe photoemission data and show that more secondary electrons are produced internally in the low-vacuum-cleaved sample than in the high-vacuum-cleaved sample. We suggest a possible explanation for this difference in the inelastic scattering.

In Figs. 46 and 47 we compare energy distributions for the high- and low-vacuum-cleaved samples. These data used the same standard for measuring quantum yield so that we may have a high degree of confidence in the relative heights of two curves at the same photon energy. Consider first the energy distributions in Fig.

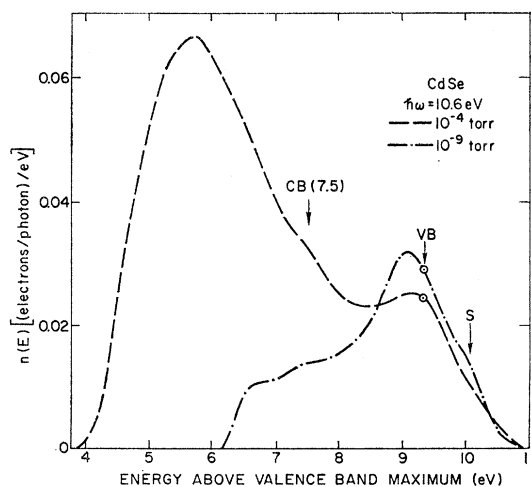


FIG. 47. Comparison of normalized energy distributions from the high-vacuum-cleaved and the low-vacuum-cleaved crystals for $\hbar\nu = 10.6$ eV.

46 for a photon energy of 8.0 eV. None of the electrons emitted at 7.3 eV has been electron-electron scattered, since the band gap is 1.8 eV. Since the heights of the two distributions are about equal at 7.3 eV, the fraction of electrons which are excited to 7.3 eV and subsequently escape the crystal is the same for the high- and low-vacuum-cleaved samples. If the threshold function at 7.3 eV is smaller for the high-vacuum cleavage (because of the larger electron affinity), then the loss of 7.3-eV electrons due to electron-electron scattering is more severe for the low-vacuum cleavage and the two effects just cancel.

Consider now the energy distributions in Fig. 47 for a photon energy of 10.6 eV. Secondary electrons may now appear at 7.3 eV since the band gap is only 1.8 eV. For $\hbar\nu = 10.6$ eV, the number of electrons emitted at 7.3 eV for the low-vacuum-cleaved sample is $2\frac{1}{2}$ times the number emitted for the high-vacuum-cleaved sample. Since we have already shown that the same fraction of 7.3-eV primary electrons escape for both experiments, the extra 150% are additional secondary electrons. Hence more secondary electrons are produced internally in the low-vacuum-cleaved sample than in the high-vacuum-cleaved sample.

It is reasonable that the electron-electron scattering probability should be greater for the low-vacuum-cleaved sample. Contamination on the surface almost certainly perturbs the crystal potential seen by an electron near the surface. One of the effects of this perturbation is to cause elastic scattering. For a fixed electron-electron mean free path, an increase in elastic scattering causes an increase in the inelastic-scattering probability.²³ The integrated path length to the surface (and hence the inelastic-scattering probability) is larger because of elastic scattering.

In summary, the photoemission data indicate that there are more secondary electrons generated internally in the low-vacuum-cleaved sample than in the high-vacuum-cleaved sample. We suggest that this increase is due to a larger electron-electron scattering probability for electrons in the low-vacuum-cleaved sample and that this increase in electron-electron scattering probability is due to the elastic scattering induced by surface contamination.

B. Estimate of Escape Depth

A knowledge of the absolute yield and the absorption coefficient allows us to estimate the escape depth for the high-vacuum-cleaved sample. It is apparent from Figs. 15 and 16 that, for $\hbar\nu > 10$ eV, most of the absorption in CdSe is to final states well above the vacuum level. This is also true for CdS (Figs. 37 and 38) and CdTe.² It follows that, regardless of the excitation process, the yield is approximately

$$Y \approx 0.5\alpha L / (1 + \alpha L). \quad (4)$$

²³ R. Stuart, F. Wooten, and W. E. Spicer, Phys. Rev. 135, A495 (1964).

This form will suffice here, even though Spicer¹⁹ has given a more exact expression for the appropriate average over the escape depths of the photoexcited electrons. T is the surface transmission probability. Of the electrons reaching the surface, a fraction T escapes into the vacuum. $\alpha L/(1+\alpha L)$ is the probability that a photoexcited electron will not be electron-electron scattered on its way to the surface. The factor of 0.5 arises since initially half of the photoexcited electrons are heading in directions away from the semiconductor surface. Equation (4) assumes that electron-electron scattered electrons are unable to escape the crystal.

In order to study the systematics of the inelastic scattering in the class of compounds CdS, CdSe, and CdTe, we shall assume a reasonable value of 0.25 for T for electrons about 8.9 eV above the top of the valence band in each material. Since the peak in the valence-band density of states occurs at about -1.3 eV, the photoexcited electrons have an average energy of about 8.9 eV for a photon energy of 10.2 eV.

For $\hbar\omega = 10.2$ eV, the absolute yield is 0.040 for the high-vacuum-cleaved sample of CdSe (Fig. 1). If we arbitrarily assume that $T = 0.25$, then $\alpha L = 0.47$. For $\hbar\omega = 10$ eV, Cardona and Harbeke¹⁷ found an absorption coefficient $\alpha = 6.2 \times 10^5$ cm⁻¹. Using this value for α , we find that the escape depth is 76 Å for an electron about 8.9 eV above the top of the valence band in CdSe.

For CdS at $\hbar\omega = 10.2$ eV, the absorption coefficient¹⁷ is 7.73×10^5 cm⁻¹, and the absolute yield of the high-vacuum-cleaved sample is 0.052 (Fig. 24). Again assuming that $T = 0.25$, the CdS escape depth is 92 Å.

For CdTe at $\hbar\omega = 10.2$ eV, the absorption coefficient²⁴ is 9.5×10^5 cm⁻¹, and the absolute yield² of the high-vacuum-cleaved sample is 0.035. The CdTe escape depth is therefore 41 Å.

In Table IV we tabulate these escape depths for CdTe, CdSe, and CdS. We find that the escape depth L decreases sharply as the band gap decreases.

VII. CONCLUSIONS

This work has explicitly demonstrated that both direct and nondirect transitions²⁵ make large contributions to the photoemission and optical properties of CdSe and CdS. We have correlated structure in the photoemission with structure in the reflectivity, thereby determining the initial and final states producing the structure in the reflectivity. Furthermore, we have

²⁴ M. Cardona, J. Appl. Phys. 36, 2181 (1965).

²⁵ In the present work the resolution of the energy distribution measurement is ~ 0.2 eV, whereas the bands have width of ~ 1.0 eV. Hence the nondirect transitions which we observe cannot be explained by transitions between very narrow bands. For a detailed discussion see Ref. 5, p. A573, and Ref. 8, p. A1044.

TABLE IV. Properties of CdTe, CdSe, and CdS for $\hbar\omega = 10.2$ eV.

Crystal	L^a (Å)	Band gap (eV)	Yield %	α (10^5 cm ⁻¹)
CdTe	41	1.6	3.5	9.5
CdSe	76	1.8	7.1	6.2
CdS	92	2.4	9.2	7.7

^a These escape depths are approximate average values for states about 8.9 eV above the valence-band maximum assuming an average surface-transmission probability (T) of 0.25.

analyzed the photoemission data to determine the nature of the transitions producing the structure in both the photoemission and reflectivity, and this information is summarized in Tables II and III. For the structure due to nondirect transitions, we have determined the optical density of states. The CdSe valence-band optical density of states is about 3.3 eV wide and consists of one peak centered at 1.3 eV below the valence-band maximum. The CdS valence-band optical density of states is about 3.0 eV wide and also peaks at -1.3 eV. The conduction-band optical density of states deduced from photoemission data involves the escape probability and inelastic-scattering probability in addition to the conduction-band optical density of states, and is therefore referred to as the conduction-band effective optical density of states (EODS). Nonetheless, peaks in the EODS usually reflect peaks in the true optical density of states. The conduction band EODS peaks near 7.5 eV for CdSe and 8.1 eV for CdS.

Using the pseudopotential calculations of Bergstresser and Cohen, we are able to locate the regions of the Brillouin zone producing most of the structure in the photoemission due to direct transitions. This is accomplished by comparing the initial and final states determined from photoemission data with the theoretical band structure. In this way we find that the regions near the zone edge connecting H and K produce the E_2 structure at $\hbar\omega \approx 7.5$ eV in CdSe and at $\hbar\omega \approx 8.0$ eV in CdS. For some weaker direct transitions also present in our data, it is not apparent which regions of the Brillouin zone are contributing. It is important to realize that the only evidence that the "direct transitions," which we observe in CdSe and CdS, are due to k -conserving transitions (as opposed to some other selection rule) is the agreement with the theoretical band structure near the zone edge connecting H and K .

The photoemission data show structure due to a deep valence band centered at about -9.9 eV in CdSe and -9.2 eV in CdS (relative to the valence-band maximum). These states have been tentatively identified as resulting from the cadmium $4d$ states.